New Phytologist

Research

Provenance legacies override species effects in shaping oak rhizosphere microbiomes and metabolomes

Sebastian Bibinger[1], Tetyana Nosenko[2], Prasath Balaji Sivaprakasam Padmanaban[2], Stefanie Schulz[1], Hilke Schroeder[3], Birgit Kersten[3], Ina Zimmer[2], Franz Buegger[2], Michael Schloter[1,4] and Jörg-Peter Schnitzler[2,5]

[1]Helmholtz Zentrum München, Research Unit Comparative Microbiome Analysis, Neuherberg, Germany; [2]Helmholtz Zentrum München, Research Unit Environmental Simulation, Neuherberg, Germany; [3]Thünen Institute of Forest Genetics, Grosshansdorf, Germany; [4]TUM School of Life Sciences, Chair of Environmental Microbiology, Technische Universität München, Freising, Germany; [5]Ecosystem Physiology, Faculty of Environment and Natural Resources, University Freiburg, Freiburg i. Br., Germany

Authors for correspondence:
Michael Schloter
Email: michael.schloter@helmholtz-munich.de

Jörg-Peter Schnitzler
Email: joergpeter.schnitzler@helmholtz-munich.de

Received: *11 November 2025*
Accepted: *7 April 2026*

New Phytologist (2026)
doi: 10.1111/nph.71213

Key words: climate change, drought tolerance, legacy effect, metabolome, microbiome, provenance, *Quercus*, rhizosphere.

Summary

- As climate change drives more frequent drought-heat extremes, selecting drought-tolerant trees is crucial for future forest resilience. However, the role of tree–microbial associations remains largely unclear. We investigated how geographic origin, species identity, and intrinsic water use efficiency (iWUE) shape the rhizosphere microbiome and root–rhizosphere metabolome of *Quercus robur* L. and *Q. petraea* (Matt.) Liebl.
- In a 6-yr common garden experiment, we analyzed trees from two distinct geographic origins (upper Rhine basin and north German lowland) using 16S/ITS metabarcoding and untargeted metabolomics.
- We found a consistent legacy effect of seed origin on the prokaryotic rhizosphere microbiome and metabolome, whereas tree species had no significant impact. The bacterial family *Pseudonocardiaceae* was enriched for trees from the drier origin (NGL), while *Blastocatellaceae* and *Micromonosporaceae* were associated with iWUE. Higher iWUE also correlated with lower prokaryotic diversity. Ellagic acid, a polyphenol associated with drought tolerance, was enriched in the drier origin. The rhizosphere fungal community, however, was largely unaffected by origin or species.
- Our findings suggest that ecotypic adaptation linked to origin can outweigh species-level traits in shaping the oak rhizosphere. These findings emphasize that provenance-driven adaptation influences plant–microbe interactions and underscore the need for provenance-aware selection to strengthen forest drought resilience.

Introduction

Forests cover *c.* 30% of Earth's land area (Hansen *et al.*, 2013) and act as biodiversity hubs as well as major global carbon sinks. In the recent decades, forests are being transformed mainly through the effects of climate change (Allen *et al.*, 2010). The speed of climate change is causing a mismatch between local tree genotypes and their environments, forcing species to shift their geographic ranges (Chen *et al.*, 2011; Loarie *et al.*, 2009). To counteract this disequilibrium, strategies such as the assisted migration of trees are being considered to align populations with future climates (Aitken & Bemmels, 2016; Zou *et al.*, 2024).

Although climate warming can promote longer growing seasons and CO_2 fertilization, it also intensifies water scarcity and leads to increased occurrence of combined drought–heat events (Manning *et al.*, 2019; Mukherjee & Mishra, 2021). This poses a significant threat to the health and stability of established forest ecosystems (Thom *et al.*, 2023). Consequently, drought tolerance is a key trait in predicting tree survival in future climates (Allen *et al.*, 2010). This complex trait involves root and leaf morphology, vascular anatomy, and the ability to rapidly acclimatize to a water deficit through processes such as solute accumulation, stomatal regulation, and partial defoliation, as well as other morphological, physiological, and molecular adjustments (Pfenninger *et al.*, 2024).

Quercus robur L. (pedunculate oak) and *Quercus petraea* (Matt.) Liebl. (sessile oak) are dominant oak species of Europe, accounting for $>9\%$ of forest trees in Germany (Thünen-Institut, 2022; Blickensdörfer *et al.*, 2024). While some oak species are considered to be drought-tolerant and may outperform other European tree species under projected warming conditions (Scharnweber *et al.*, 2011), both provenance and species traits shape their responses to drought (Bruschi, 2010; Arend *et al.*, 2011; Kuster *et al.*, 2013; Rabarijaona *et al.*, 2022). Compared with *Q. robur*, *Q. petraea* tends to occupy drier, well-drained sites and shows higher intrinsic

water use efficiency (iWUE) (Ponton *et al.*, 2001, 2002; Nosenko *et al.*, 2025).

iWUE, as estimated by the $\delta^{13}C$ value, is an index of carbon gain relative to water loss and can serve as a proxy for drought tolerance (Farquhar *et al.*, 1989; Nosenko *et al.*, 2025). Greater stomatal responsiveness to declining humidity has also been reported in *Q. robur* (Gieger & Thomas, 2005). Across German oak populations, differences in $\delta^{13}C$ correlate with climate/soil water availability at the origin, suggesting constitutive adaptation. These differences are particularly evident under extreme drought, reflecting phenotypic plasticity (Nosenko *et al.*, 2025). This suggests a genetic basis for adaptation and aligns with evidence of a small number of large-effect genes with contrasting expression patterns between high- and low-iWUE oak genotypes (Brendel *et al.*, 2008; Le Provost *et al.*, 2022).

Belowground tree–microbiota interactions may contribute to the mediation of drought response. Generally, the rhizosphere microbiome, comprising bacteria, archaea, fungi, and protists, plays a pivotal role in plant nutrition, disease resistance, and abiotic stress tolerance (Bulgarelli *et al.*, 2013; Trivedi *et al.*, 2020). It can enhance drought tolerance by improving water and nutrient acquisition, modulating hormonal signaling, altering root system architecture, and priming plant stress responses (Augé, 2001; Rolli *et al.*, 2015; Vurukonda *et al.*, 2016; Pereira *et al.*, 2020; Carter *et al.*, 2023). During drought, microbial communities often shift toward stress-tolerant taxa or into drought-resilient mycorrhizal assemblages (Lekberg *et al.*, 2012; Naylor & Coleman-Derr, 2018).

The rhizosphere microbiome assembly is shaped by plant-controlled exudation patterns (Koprivova & Kopriva, 2022; Wang *et al.*, 2024) and varies among species (Ishida *et al.*, 2007; Wang & Sugiyama, 2020) and even within genotypes of the same host species (Whitham *et al.*, 2012). Genotype effects on associated microbiomes have been observed in annual and perennial species (Schlaeppi *et al.*, 2014; Wagner *et al.*, 2016; Brown *et al.*, 2020; Simonin *et al.*, 2020; da Costa *et al.*, 2022), including trees, for example, *Populus* spp., *Picea* spp., and *Pinus radiata* (Velmala *et al.*, 2013; Lamit *et al.*, 2016; Gallart *et al.*, 2018; Li *et al.*, 2018; Bonito *et al.*, 2019). Furthermore, provenance-related 'origin legacy' effects, a lasting imprint of the plant origin on their microbiome, were reported to shape root-associated microbiomes in *Pinus sylvestris*, *Betula pendula*, and *Fokienia hodginsii* (Färkkilä *et al.*, 2023; Liu *et al.*, 2024; Maitra *et al.*, 2024). Notably, seed-borne (vertical) transmission can introduce microbiota to the next generation (Abdelfattah *et al.*, 2021; Seitz *et al.*, 2022), potentially interacting with horizontal recruitment from the soil. In fact, seed microbiomes are increasingly recognized as a primary source of inoculum for plant holobionts (Shade *et al.*, 2017; U'Ren & Zimmerman, 2021; Simonin *et al.*, 2022).

Nevertheless, the links between traits and the microbiome that underlie drought adaptation in long-lived trees have not yet been sufficiently explored. Due to their perennial nature, genotypic effects in trees are likely to be more persistent and cumulative than in annual plants, in which such influences may be reset each season. A tree's geographic origin might therefore have a long-lasting impact on the rhizosphere microbial composition and chemistry, on the one hand by genetic adaptation and on the other hand by vertical transmission of microbes related to important traits, for example, drought tolerance. Furthermore, interactions between drought-adaptive traits of the tree, such as iWUE, and the diversity or composition of rhizosphere microbiomes are largely unknown.

In this study, we examine how the origin (differing in mean annual precipitation) of the tree (ecotype), species identity, and iWUE influence the rhizosphere microbiome and metabolome of *Q. robur* and *Q. petraea* trees grown from seeds in a common soil for over 6 yr. Using $\delta^{13}C$-based leaf iWUE alongside untargeted root–rhizosphere metabolomics and amplicon sequencing of rhizosphere fungi and prokaryotes, we evaluate two hypotheses:
(**1**) The oak rhizosphere retains origin-specific signatures in fungal and prokaryotic microbiomes and metabolomes even after several years of growth in a shared substrate and environment.
(**2**) Variation in iWUE, reflecting the capacity of a tree to adapt to different environmental conditions, is linked to the associated rhizosphere microbiome composition.

Materials and Methods

Experimental setup

This study included a total of 109 trees from two oak species, *Quercus robur* (L.) and *Q. petraea* (Matt.) Liebl (56 and 53 trees, respectively) grown in the common garden area at the Thünen Institute for Forest Genetics, Grosshansdorf, Germany (FG), as described elsewhere (Nosenko *et al.*, 2025). Briefly, 2-yr-old plants were bought from the tree nursery Schrader Pflanzen Handelsgesellschaft GmbH & Co., Kölln-Reisiek, Germany in 2019. The seeds used by the nursery to raise the young trees originated from two forest sites located in the upper Rhine basin (URB; 49.014° N, 8.156° E) and the northeast German lowlands (NGL; 54.144° N, 13.072° E), respectively.

Climate information and climate-derived soil parameters were obtained from the DWD Open Data Portal (https://opendata.dwd.de) as described in Nosenko *et al.* (2025). Moisture deficit (MD) was calculated as the difference between mean annual evaporation over grass and loamy sand and mean annual precipitation.

The full origin descriptions can be found in the Supporting Information (Table S1). The two regions differ in their average annual precipitation (803 mm and 657 mm at upper Rhine basin (URB) and north German lowland (NGL), respectively), soil water-holding capacity measured within the effective rooting depth of up to 1 m during the vegetation period (307.15 mm and 254.74 mm in URB and NGL, respectively), and MD (−419.3 and −292.0 in URB and NGL, respectively) (Nosenko *et al.*, 2025).

Seeds that had not been surface-disinfected were germinated, and the seedlings were grown in open ground in a common substrate at the tree nursery. In March 2019, bare-rooted seedlings were planted to 3-l pots filled with standard forest soil mixture (Table S2) and arranged in a randomized block design in a

common garden setup and maintained under mesic conditions with supplemental irrigation at the outdoor area. In the winter of 2021, all seedlings were repotted into 15-l pots using fresh substrate of the same composition as before. To differentiate between *Q. robur* and *Q. petraea* and exclude hybrid genotypes from the study, molecular marker analysis was conducted on all trees in the common garden as described before (Schroeder & Kersten, 2023). In June 2020, three leaves were collected from the sun-exposed part of the canopy of each of the 109 seedlings from the two populations, snap-frozen in liquid nitrogen, and stored at −80°C for further assessment of iWUE (will be discussed later).

Thirty-six oaks (18 trees from species *Q. robur* and *Q. petraea*, respectively) were selected from two origins (20 from NGL and 16 from URB) (Fig. 1) based on leaf carbon isotope ratio (δ13C) values. Four to five trees with the lowest and four to five trees with the highest δ13C values in both solid and soluble leaf fractions were selected from each species and population. The uneven sample sizes reflect the fact that only eight *Q. petraea* remained in the URB population after the exclusion of hybrids. Because no significant variance was observed in the difference between δ13C in the soluble and solid fractions between individual trees, we used only δ13C in the soluble fraction for calculating iWUE in the subset of trees selected for further analyses. The resulting selection covered iWUE values in the range from 57.7 to 116.4 μmol mol^{-1}. Root samples were collected in February 2023 from the 6-yr-old plants. Plants were removed from their pots, and roots were sampled from the lower third of the root ball using scissors (Fig. S1). The cuttings, with soil still attached, were placed in aluminum bags, immediately flash-frozen in liquid nitrogen, and stored at −70°C until further processing. In 2022, tree height and basal stem diameter were comparable across all origins and species.

iWUE determination

We used iWUE as a proxy for the tree's drought tolerance. iWUE was estimated based on the stable carbon isotope ratio ($\delta^{13}C$). Three leaves collected in 2020 from each of the 109 seedlings were ground and pooled. ^{13}C stable isotope analysis was performed in soluble and solid fractions of the leaf tissue using an Isotope Ratio Mass Spectrometer (delta V Advantage, ThermoFisher, Dreieich, Germany) and an Elemental Analyzer Euro EA (Eurovector, Milano, Italy) following established procedures (Simon *et al.*, 2013; Nosenko *et al.*, 2025). $\delta^{13}C$ values are expressed relative to the international Vienna Pee Dee Belemnite (VPDB) standard:

$$\delta^{13}C\ [‰VPDB] = \left(\frac{\left(R_{sample} - R_{VPDB}\right)}{R_{VPDB}}\right) \times 1000$$

where R_{sample} is the $^{13}C:{}^{12}C$ ratio of the sample and $R_{VPDB} = 0.0111802$ (Werner & Brand, 2001). iWUE values were then calculated from $\delta^{13}C$ in the soluble fractions of leaf extracts using the R package ISOCALCR (Mathias & Hudiburg, 2022). For that, mean temperatures for the period of leaf development (16.04–15.06.2020) were calculated from the daily temperature information of the German Weather Service station 1975 (Opendata.Dwd.de). Atmospheric carbon isotope ratios ($\delta^{13}Catm$) were obtained from the atmospheric CO_2 and $\delta^{13}Catm$ database (Belmecheri & Lavergne, 2020). $\delta^{13}C$ and iWUE for all selected trees can be found in Table S3.

Sample preparation

Root-soil samples were shaken while frozen to separate soil particles from roots, with some residual soil remaining attached to the

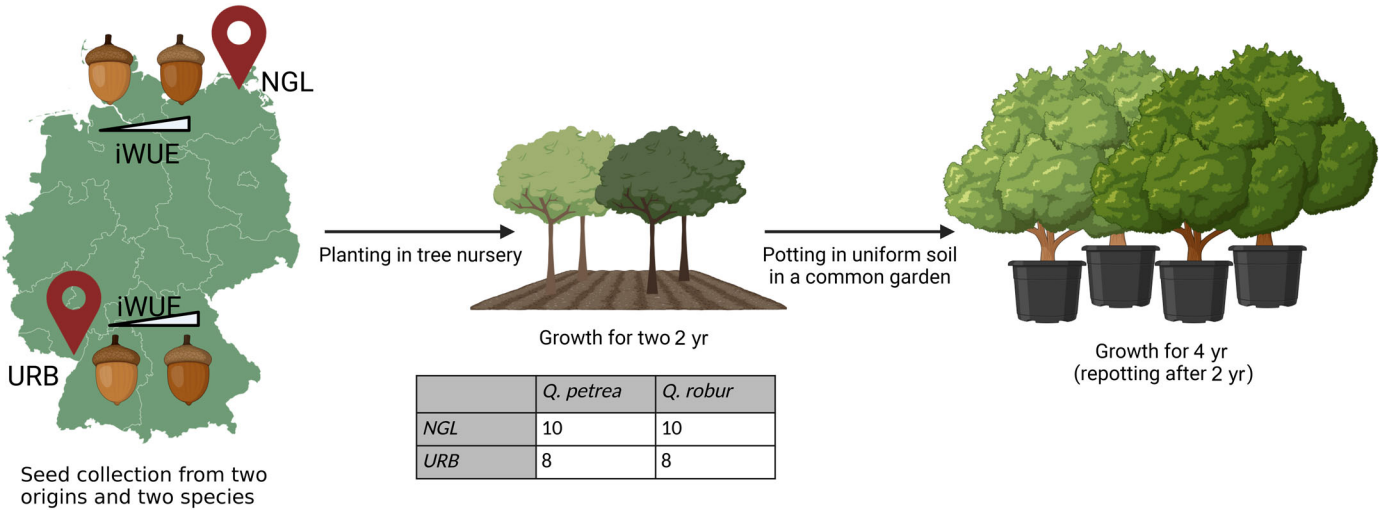

	Q. petrea	*Q. robur*
NGL	10	10
URB	8	8

Fig. 1 Graphical representation of experimental setup. *Quercus* spp. seeds were collected at two origins, upper Rhine basin (URB) and north German lowland (NGL). Seeds were then grown for 2 yr in a tree nursery before planting in a common garden. After an additional 4 yr of growth, rhizosphere samples were collected in 2023. Intrinsic water use efficiency was determined in 2020. Map lines delineate study areas and do not necessarily depict accepted national boundaries. Created in BioRender. Bibinger, S. (2026) https://BioRender.com/j959b0o.

roots. Both fractions were freeze-dried; separated soil was used for microbiome sequencing (see 'LC-MS analysis' in the Materials and Methods section), and roots were ground to a fine powder for metabolite extraction following Bertić *et al.* (2021) and Sivaprakasam Padmanaban *et al.* (2025). Briefly, 50 mg powder was extracted with 1 ml ice-cold methanol : 2-propanol : water (1 : 1 : 1, v/v/v), vortexed (30 s), sonicated (10 min, 4°C), and centrifuged (10 000 ***g***, 10 min, 4°C). Supernatants were vacuum-dried and reconstituted in 200 µl 50% acetonitrile.

LC-MS analysis

Untargeted metabolite profiling of root–rhizosphere samples was performed as described by Hemmler *et al.* (2018) and Ghirardo *et al.* (2020) using an Ultimate 3000RS UPLC coupled to a Bruker Impact II UHR QqToF MS with an Apollo II ESI source (Bruker Daltonics, Bremen, Germany). To provide broad compound coverage, nonpolar and polar metabolites were analyzed using complementary reversed-phase liquid chromatography (RPLC) and hydrophilic interaction liquid chromatography (HILIC) methods, with the MS operated in ESI- for RPLC and ESI+ for HILIC. As this study employs nontargeted LC-MS/GC-MS metabolomics, absolute metabolite concentrations (e.g. µM or mg l^{-1}) were not determined. Instead, metabolites were detected as analytical features defined by their *m/z* and retention time and quantified based on instrument response, reported as peak area or peak height (signal intensity/ion counts) in arbitrary units.

Mobile phases for both LC methods were Solvent A (Water Lichrosolv® containing 0.1% (v/v) formic acid) and Solvent B (Acetonitrile Honeywell® containing 0.1% (v/v) formic acid). Nonpolar metabolites were separated using RPLC on an Acquity BEH C18 column (Waters, Eschborn, Germany; 150 mm × 2.1 mm, 1.7 µm) with the following gradient: 0–1 min 95% A; 1–15 min 95–70% A; 15–17 min 70–20% A; 17–20 min 20% A; 20–22 min 20–0.5% A; 22–27 min 0.5% A; 27–29 min 0.5–95% A; 29–31 min 95% A. Polar metabolites were separated using HILIC on an Acquity BEH Amide column (Waters; 100 mm × 2.1 mm, 1.7 µm) with the following gradient: 0–1 min 5% A; 1–16 min 5–30% A; 16–18 min 30–80% A; 18–19 min 80% A; 19–20 min 80–95% A; 20–21 min 95–4.5% A. For both chromatographic methods, flow rate (0.4 ml min^{-1}), column temperature (40°C), and injection volume (5 µl) were constant.

To control for analytical stability and potential spectrometric biases, the injection sequence was randomized. Quality control samples were prepared by pooling equal volumes of all root extracts and were injected every five study samples. Solvent blanks were injected at the beginning and end of each batch to assess background signals and carryover.

MS calibration, acquisition, and MS/MS

Mass spectrometry was performed after calibration with a mixture of 50 ml water, 50 ml 2-propanol, 1 ml NaOH, and 200 µl formic acid. The MS settings were as follows: nebulizer pressure 2.0 bar, dry gas flow 8.0 $l \cdot min^{-1}$, dry gas temperature 200°C, capillary voltage 4500 V (positive mode) or 3500 V (negative mode), and endplate offset 500 V. Spectra were recorded over a mass range of *m/z* 20–2000. Metabolite identification was supported by tandem MS in auto MS/MS acquisition mode with smart exclusion; precursor ions were selected when the difference between the rolling average and actual spectra exceeded 1000 counts, and fragmentation was performed in the collision cell with collision energies ranging from 5 to 20 eV.

Raw data were processed and analyzed using the METABOSCAPE software (v.4.0, Bruker). Initial feature finding used a minimum intensity of 1000 counts per spectrum and a minimum peak length of seven spectra. This was followed by recursive feature extraction requiring a minimum feature length of six spectra and presence in at least two out of five samples. The workflow included peak picking, alignment, isotope filtering, and grouping of features via peak-area correlations. To enhance feature identification, ionization settings for both positive and negative modes were configured by defining primary, seed, and common ions. Before normalization, blank subtraction was performed to remove background signals originating from solvents, reagents, and the analytical system; features detected in procedural blanks were subtracted from sample signals (or removed if predominantly present in blanks). Metabolite data were $\log_{10}$-transformed and Pareto-scaled before statistical analysis using the package IMIFA v.2.2.0 (Murphy *et al.*, 2020) to compress high-abundance outliers, improve approximate normality, and avoid model overfitting. After blank correction, remaining missing values were imputed with random numbers below the detection limit (range 1–800).

Metabolite annotation was performed using a hierarchical approach. High-confidence identification was achieved by matching experimental MS/MS spectra against HMDB, MoNa, and the Vaniya/Fiehn Natural Products Library. For mass features without a library match, a putative annotation was assigned using the software's 'smart formula' generation based on elemental ratios and accurate mass (*m/z*). While these formulas were subsequently verified against an in-house R-based script and metabolite database (Bertić *et al.*, 2021), only the chemical formula itself was used in subsequent steps to avoid potential misidentification. Chemical classification of significant features was carried out using Multidimensional Stoichiometric Compound Classification, based on elemental composition and ratios including C, N, H, O, P, S, O : C, N : C, H : C, P : C, and N : P (Rivas-Ubach *et al.*, 2018).

Microbiome analysis

DNA was extracted from *c.* 0.5 g of root-free rhizosphere soil using the NucleoSpin Soil kit (Macherey-Nagel, Düren, Germany) with buffer SL1 and enhancer SX following the manufacturer's instructions. For this purpose, bead beating was performed using a Precellys 24 tissue homogenizer (Bertin Instruments, Frankfurt am Main, Germany). Quality of the extracted DNA was assessed photometrically by a NanoDrop 1000 spectrophotometer (ThermoFisher Scientific, Germering, Germany), and DNA quantity was determined using the Quant-iT PicoGreen dsDNA Assay Kit

(ThermoFisher Scientific) with a Spark® Multimode Microplate Reader (Tecan Trading AG, Männedorf, Switzerland).

As recommended by the Earth Microbiome Project (earthmicrobiome.ucsd.edu), we used the primer pair 515FB-806RB (Apprill *et al.*, 2015; Parada *et al.*, 2016) for amplification of the V4 region of the 16S rRNA gene (from now 16S) and primers ITS3/ITS4 (White *et al.*, 1990) for the amplification of the fungal rRNA gene region (from now ITS).

The PCR for both target regions was performed in a 25 µl total volume, consisting of 5 ng of template DNA, 12.5 µl NEBNext high-fidelity polymerase (New England Biolabs, Frankfurt am Main, Germany), 0.3 pmol per primer, and 2.5 µl of 3% BSA. PCR conditions were as follows: 1 min at 98°C; 25 cycles (16S) and 28 cycles (ITS) of 10 s at 98°C, 30 s at 55°C, and 30 s at 72°C; 5 min at 72°C. To confirm successful amplification, 1% (w/v) agarose gel electrophoresis was used. Amplified DNA was then purified using MagSI NGSprep Plus Beads (Magtivio, the Netherlands) at a ratio of 0.8 : 1 beads/PCR product. DNA quantity was again determined by Quant-iT PicoGreen dsDNA Assay Kit with a Spark® Multimode Microplate Reader.

For both 16S and ITS, sequencing indices were added to the PCR products by PCR using the Nextera XT Index Kit v2 (Illumina, Inc., München, Germany) in a total volume of 25 µl, consisting of 10 ng template DNA, 12.5 µl NEBNext high-fidelity polymerase, and 2.5 µl of each indexing primer. The PCR conditions were as follows: 30 s at 98°C; 8 cycles with 10 s at 98°C, 30 s at 55°C, 30 s at 72°C; 5 min at 72°C. PCR products were again purified with MagSI NGSprep Plus Beads. The final DNA quantification was performed through capillary electrophoresis using the 5200 Fragment Analyzer (Agilent, Waldbronn, Germany). Samples were then pooled equimolarly at 4 nM and sequenced on an Illumina MiSeq using the Reagent Kit v3 (Illumina, Inc.). In total, 3935 957 and 2639 845 reads were obtained for 16S and ITS sequencing, respectively.

Sequencing adapters were removed from demultiplexed raw sequences using CutAdapt v.3.5 (Martin, 2011). Read processing was performed using DADA2 v.1.34.0 (Callahan *et al.*, 2016) and R v.4.4.2 (R Core Team, 2024) in R Studio v.2023.09.1 (RStudio Team, 2020). 16S reads were trimmed at 260 bp (forward) and 200 bp (reverse). ITS reads were trimmed at 250 bp (forward) and 209 bp (reverse) and quality filtered using 'maxEE = (2,2)'. Filtering parameters were selected after extensive testing of variable-length trimming approaches, which proved unsuitable for this dataset due to a technical trade-off between sequence quality and successful paired-end merging. Resulting amplicon sequence variants (ASV) sequences were taxonomically classified using the SILVA database v.138.1 (Quast *et al.*, 2013) for 16S sequences and UNITE database v.10.0 (Abarenkov *et al.*, 2024) for ITS sequences. Read numbers throughout the DADA2 pipeline are provided in Table S4 (16S) and Table S5 (ITS). Mitochondrial, chloroplast, and singleton reads were excluded from further analysis. Decontamination was carried out using Decontam v.1.22.0 (Davis *et al.*, 2017). Contaminants were defined based on their prevalence in negative controls using a strict threshold of $P < 0.05$. Appropriate sequencing depth was assessed through rarefaction curves using the vegan package v.2.6.10 (Oksanen *et al.*, 2025). Detailed information about specific read numbers can be found in Tables S4 (16S) and S5 (ITS). Samples were normalized using cumulative sum scaling from the package metagMisc v.0.5.0 (Mikryukov, 2025). Fungal guild assignment was performed to identify ectomycorrhizal (ECM) taxa given their critical role to the host trees using the FUNGuild database (Nguyen *et al.*, 2016) and the FUNGuildR v.0.3.0 package (Furneaux, 2020).

Statistical analysis

All subsequent statistical analyses were performed with R v.4.4.2 (R Core Team, 2024) and RStudio v.2023.09.1 (RStudio Team, 2023). Unless specified differently, analyses were performed using phyloseq v.1.50.0. Data were visualised using ggplot v.3.5.1 (Wickham, 2016), viridis v.0.6.5 (Garnier *et al.*, 2024), and ggpubr v.0.6.0 (Kassambara, 2023). Statistical significance was established at $P \leq 0.05$.

16S and ITS Shannon diversity and ASV richness were calculated using *phyloseq*. To determine 16S and ITS evenness, the package microbiome v.1.28.0 (Lahti & Shetty, 2017) was used. Metabolome diversity was determined as microbiome diversity, but metabolite reads below the detection limit (0–800 reads) were set to zero beforehand. Significance of differences in diversity indices and metabolite abundances were tested using ANOVA or Sheirer–Ray–Hare tests. 16S and ITS community composition was visualized in stacked bar plots using the package microeco v.1.13.0 (Liu *et al.*, 2021). Beta-diversity was estimated based on Bray–Curtis dissimilarities calculated at the ASV level. Nonmetric multidimensional scaling (NMDS) and Permutational Multivariate Analysis of Variance (PERMANOVA) were performed using the package vegan v.2.6.10 (Oksanen *et al.*, 2025) The PERMANOVA model included the interaction terms for origin, species, and iWUE (~ origin * species * iWUE). Statistical significance was assessed using Type I sum of squares with 999 permutations. To ensure that differences in group dispersion did not confound PERMANOVA results, we evaluated betadispersion to confirm homogeneity of variances beforehand.

Differentially abundant microbial families between origins, species, and along iWUE were identified using the DESeq2 v.1.48.1 package (Love *et al.*, 2014) with Benjamini–Hochberg (BH) false discovery rate correction. Pairwise contrasts were defined to compare *Q. robur* vs *Q. petraea* (reference) and origin URB vs origin NGL (reference) (Kembel *et al.*, 2010).

Orthogonal Partial Least Squares Discriminant Analysis (OPLS-DA) was performed to separate predefined sample groups, making it easier to find biomarkers from the metabolite data using the R package ropls v.1.40.0 (Thevenot *et al.*, 2015). Initially, metabolites were selected based on an OPLS-DA VIP (Variable Importance in Projection) score greater than 1.0, a P-value < 0.05, and an absolute $\log_2$ fold change > 1.0, ensuring that only biologically relevant biomarkers with significant abundance differences were retained. The selected metabolite data were then $\log_{10}$-transformed and Pareto-scaled to compress high-abundance outliers, stabilize variance, and prevent overfitting.

New Phytologist

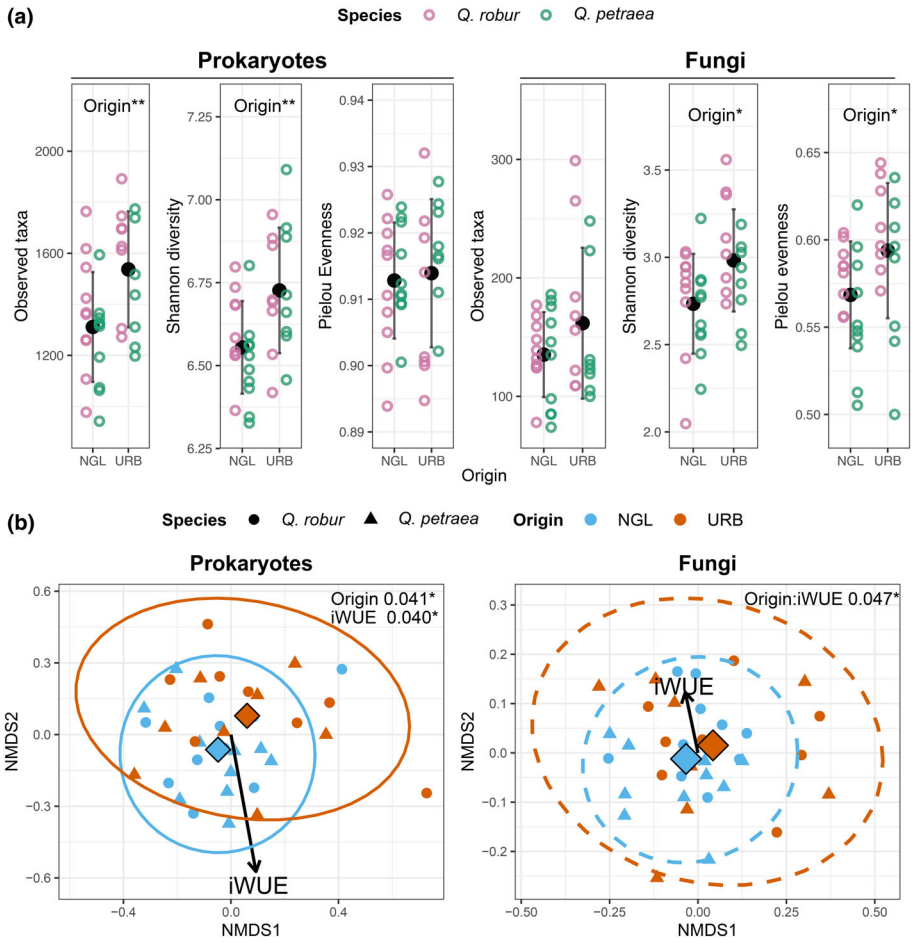

Fig. 2 Effects of origin (upper Rhine basin, URB; north German lowland, NGL), species and intrinsic water use efficiency (iWUE) of *Quercus* spp. on prokaryotic and fungal microbiome diversity and structure. (a) Alpha diversity found in the rhizosphere split by origin and species. Richness, Shannon diversity, and Pielou evenness were used to assess alpha diversity. Significant factors as determined by analysis of variance (ANOVA) are noted in the plot. For visual clarity, the *y*-axis was constrained, hiding one outlier in prokaryotic richness and one in fungal evenness. Error bars indicate SD. (b) Nonmetric multidimensional scaling (NMDS) based on Bray–Curtis distances was used to assess β-diversity. The arrows indicate the direction of increasing iWUE. Diamond shapes represent the origin centroids. Significant main effects (Prokaryotes) or significant interaction terms (Fungi: Origin: iWUE) as determined by permutational multivariate analysis of variance (PERMANOVA) are shown in the plot with a '*'. Solid lines indicate significant results ($P \leq 0.05$), while dotted lines represent non-significant trends. The full results from the PERMANOVA model can be found in the supplement (Supporting Information Table S8).

Global congruence between microbiome and metabolome was evaluated via Procrustes analysis using the vegan package. PCA ordinations of both datasets were compared using Procrustes analysis and significance was tested with 999 permutations.

For the correlation analysis, microbiome data were first transformed using a centered log-ratio (clr) transformation via the COMPOSITIONS package v.2.0.8 (van den Boogaart *et al.*, 2024). Correlations between ASVs and metabolites were then calculated using HMISC v.5.2–3 (Harrell Jr, 2026). Correlations with Spearman's rho > 0.6 were used to generate a correlation network using IGRAPH v.2.1.4 (Antonov *et al.*, 2023).

All statistical parameters, including test statistics, exact p-values, and degrees of freedom for alpha and beta diversity analyses as well as correlations, are provided in Table S6.

The R scripts for analysis were formatted, refactored, and debugged with assistance from the large-language model Gemini (Google LLC, Hamburg, Germany). AI-generated code was always manually reviewed, validated, and adapted.

Results

Origin-based legacies persist after 6 yr in common soil

Prokaryotic α-diversity and β-diversity show origin effects We retrieved an average of 65 555 high-quality reads per sample from 16S rRNA gene metabarcoding. This was sufficient for covering the present biodiversity, as shown by rarefaction curves (Table S4; Fig. S2a). Across all 36 samples, we obtained 10 203 unique ASVs, of which 10 177 were assigned to bacteria and 26 were assigned to archaea. A total of four ASVs were identified as contaminants and removed before downstream analysis (Table S7). The bacterial community was dominated by members of the phyla *Pseudomonadota*, with an average relative abundance of 35.5% (±2.2% SD), *Actinomycetota* (16.5% ± 3.1%), *Acidobacteriota* (12.9% ± 1.4%), and *Chloroflexota* (9.4% ± 2.1%) throughout the samples. The most prominent families included *Xanthobacteraceae* (5.2% ± 0.7%), *Nitrosomonadaceae* (3.3% ± 0.9%), and *Pirellulaceae* (3.0% ± 0.6%) (Fig. S3a,b).

ASV richness, Shannon index, and Pielou's evenness metric were determined to investigate the microbial alpha diversity (Fig. 2a). There were no differences in ASV richness or Shannon diversity between the two species. However, differences in diversity were observed between tree origins. Prokaryotic microbiomes from origin URB showed higher ASV richness (mean ± SD: 1603 ± 343) and Shannon diversity (6.73 ± 0.19) than microbiomes from NGL (Observed: 1311 ± 216; Shannon: 6.54 ± 0.15) at statistical significance ($P_{observed} = 0.001$; $P_{shannon} = 0.004$, see Table S6, for full statistical details). If splitting the data by tree species, a subsequent Wilcoxon test confirmed the statistical significance of origin, only for prokaryotic Shannon diversity within *Q.*

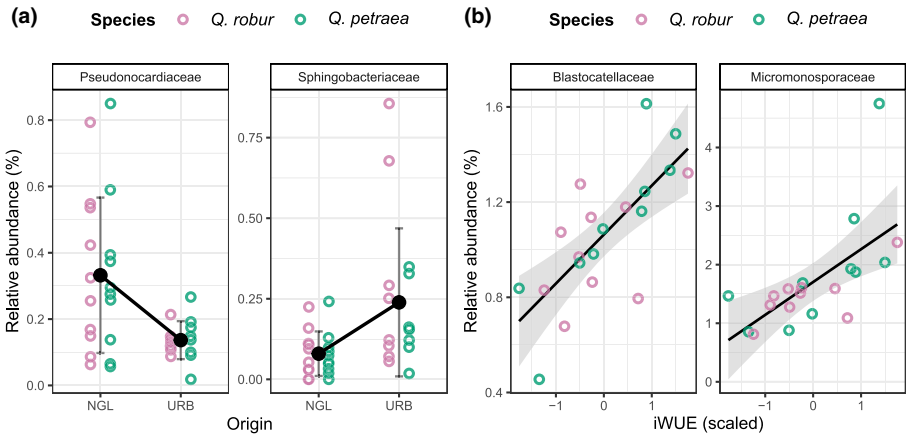

Fig. 3 Abundance of prokaryotic families in the rhizosphere of *Quercus* spp. showing significant response to origin or intrinsic water use efficiency (iWUE) as found through DESeq2 analysis. (a) Families associated with one of the origins (upper Rhine basin, URB; north German lowland, NGL). Error bars indicate SD. (b) Families associated with iWUE.

robur, which showed a significant difference between NGL and URB ($P = 0.009$). Prokaryotic Pielou's evenness was generally comparable between origins and species. No significant differences in alpha diversity were found between *Q. robur* and *Q. petraea* when analyzed within each origin individually.

PERMANOVA based on Bray–Curtis distances revealed compositional differences in the prokaryotic communities of trees originating from URB and NGL (Fig. 2b). Although the effect size was small ($R^2 = 0.04$), the difference was significant ($P = 0.024$; see Table S8, for the full PERMANOVA model). No compositional differences in the prokaryotic communities between tree species were detected ($P = 0.662$). To pinpoint specific taxa driving the observed differences, we performed a differential abundance analysis using DESeq2. While we could not find differentially abundant ASVs, a family-level analysis revealed an accumulative effect which resulted in significant enrichment of *Pseudonocardiaceae* in origin NGL ($\log_2$FC $= -1.27$, $P = 0.014$, predominately genera *Amycolatopsis* and *Pseudonocardia*), and *Sphingobacteriaceae* ($\log_2$FC $= 1.68$, $P = 0.014$, predominately genera *Pedobacter* and *Mucilaginibacter*) in origin URB (Fig. 3a). Consistent with our PERMANOVA results, no differentially abundant families or ASVs were found between the tree species.

Fungal alpha but not beta diversity shows origin effects From ITS sequencing, we received 35 098 high-quality reads per sample, representing 1902 unique ASVs, which also covered fungal biodiversity sufficiently (Table S5; Fig. S2b).

Fungal communities displayed a higher variability in their composition. Dominating phyla were *Ascomycota* (62.8% ± 13.3%) and *Basidiomycota* (31.4% ± 13.1%), together accounting for *c.* 94.0% of the total fungal sequences. Highly abundant fungal families, besides unclassified families from the phylum *Ascomycota*, include the ECM family *Sclerodermataceae* (27.1% ± 13.1%), *Gymnoascaceae* (7.8% ± 5.1%), and *Pseudeurotiaceae* (5.8% ± 4.4%) (Figs S3c,d). We included an assessment of fungal guild assignment using the Funguild database. The most prominent guilds identified were ECM and undefined saprotrophs (Fig. S4). The ECM community was dominated by *Scleroderma areolatum* (76.2%) and *Scleroderma verrucosu* (9.6%).

Fungal ASV richness showed no significant difference between origins or species (Fig. 2a). However, NGL fungal communities exhibited significantly lower Shannon diversity than URB communities (2.73 ± 0.29 vs 2.98 ± 0.29; $P = 0.036$), which was driven by the same pattern in Pielou's evenness (0.56 ± 0.04 vs 0.59 ± 0.04; $P = 0.014$). Again, subsequent Wilcoxon tests for origin effects within each tree species separately did not confirm any significant differences between origins. Similarly, no significant differences in alpha diversity were found between *Q. robur* and *Q. petraea* within each origin.

Fungal composition was not significantly different between tree species or origins ($P = 0.493$ and 0.077), as determined through PERMANOVA (Fig. 2b). However, the interaction between origin and iWUE had a significant effect on fungal microbiome composition ($R^2 = 0.047$, $P = 0.014$). We found no significant impacts of any factors on the ECM subcommunity. Consistent with our PERMANOVA results, no differentially abundant families or ASVs were found between the tree species or origins using DESeq2.

Metabolomes are separated by origin and differ in their class composition Across all samples, 1071 metabolites were identified and assigned to six classes: carbohydrates, lipids, amino sugars, nucleotides, proteins, and oxyaromatic compounds. Metabolite richness, Shannon index, and Pielou's evenness metric were determined to investigate the metabolite alpha diversity (Fig. 4a). Metabolite richness was significantly higher in samples from origin NGL than from URB (701 ± 95 and 624 ± 100, ANOVA $P = 0.02$). Similar results were found for Shannon diversity (5.65 ± 0.10 and 5.53 ± 0.18, $P = 0.02$). Metabolite evenness, on the other hand, was significantly higher in *Q. petraea* than in *Q. robur* (0.87 ± 0.01 and 0.86 ± 0.01, $P = 7e\text{-}06$).

To investigate compositional differences between the tree origins and species, we performed an OPLS-DA. While a model for the factor origin could be constructed, no significant predictive or orthogonal components could be identified for the factor tree species. For the factor origin, OPLS-DA showed a clear separation in metabolites between NGL and URB (Fig. 4b). The model accounted for 90.7% of the variation in the response variable

New Phytologist

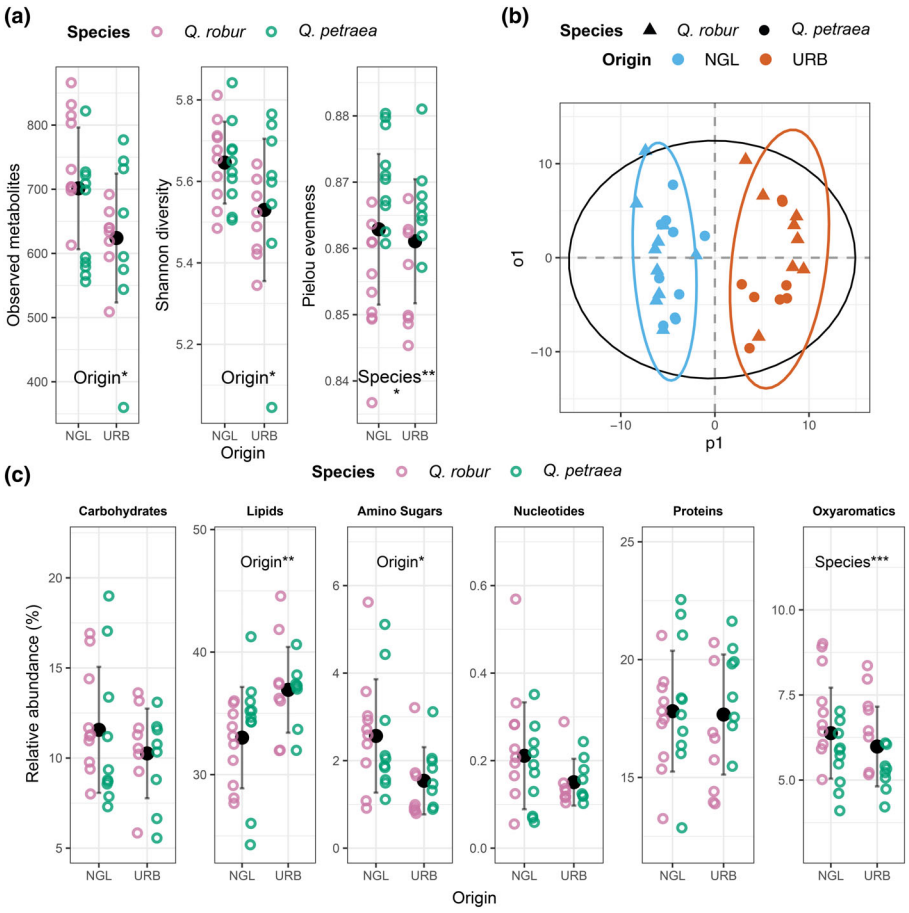

Fig. 4 Effects of origin, species, and intrinsic water use efficiency (iWUE) of *Quercus* spp. on rhizosphere metabolome composition. (a) Metabolome Shannon diversity split by tree origin and species. Significant differences as determined by analysis of variance (ANOVA) are displayed. (b) Orthogonal Partial Least Squares Discriminant Analysis scores plot discriminating metabolomes upper Rhine basin (URB) and north German lowland (NGL). (c) Metabolite class relative abundance per species and origin. Significant differences, as found by ANOVA, are marked in the plot with a '*'. Error bars indicate SD.

(R^2Y) and 19.3% of the variation in the predictor variables (R^2X) and showed strong predictive performance ($Q2 = 0.648$, $P = 0.05$). A total of 58 metabolites were identified as key drivers of the separation between origins, meeting the criteria of a VIP score > 1, log-fold change ($\log_2$FC) > 1, and P-value < 0.05. The abundance of these 58 metabolites and their classification can be found in Fig. S5 and Table S9. Five key metabolites (two lipids, two proteins, and one unmatched compound) were enriched in origin URB, while 53 metabolites were enriched in origin NGL. The top 10 metabolites with the highest VIP score included five lipids, three proteins, and one plant-derived oxyaromatic mass feature classified as ellagic acid. Ellagic acid with a VIP score of 3.49 was enriched in the rhizosphere of NGL with a $\log_2$ fold change of 2.69 ($P < 0.01$). Concerning overall metabolite classes, we found comparable carbohydrate abundance between tree species and origins (Fig. 4c). For lipids, samples from origin URB showed a significantly higher abundance (36.9% ± 3.5%) than those from NGL (33.0% ± 4.1%), as determined by ANOVA ($P = 0.006$). An opposite trend was observed for amino sugars, which showed significantly higher abundance in samples from NGL (2.6% ± 1.3%) than in samples from URB (1.5% ± 0.8%, ANOVA $P = 0.010$). While nucleotide and protein abundance were comparable between species and origins, samples from *Q. robur* contained significantly higher amounts of oxyaromatic compounds (6.9% ± 1.3%) than *Q. petraea* (5.4% ± 0.8%, ANOVA $P < 0.001$). Overall, 27.9% of the metabolites could not be assigned to a class.

Microbiome–metabolome coupling is limited globally but reveals shared hubs

A Procrustes analysis of the PCA scores was used to assess global congruence between microbiome and metabolome profiles. On the one hand, no significant association was found for either prokaryotes or fungi (prokaryotes: Procrustes $r = 0.257$, $P = 0.16$; fungi: $r = 0.2544$, $P = 0.18$). On the other hand, there was a significant negative correlation between metabolite and prokaryotic Shannon diversity (rho = −0.46, $P = 0.006$, Fig. S6), which did not extend to fungal diversity (rho = −0.08, $P = 0.649$).

Specific microbe–metabolite relationships emerged between the 58 key metabolites and members of the prokaryotic and fungal microbiomes (Fig. 5).

Correlation networks were constructed, with edges representing significant correlations (rho > 0.4) between metabolites and prokaryotic (Fig. 5a) or fungal ASVs (Fig. 5c). The prokaryotic network contained 234 nodes and 408 edges with 55.9% positive edges. The fungal network contained 76 nodes and 208 edges with 67.8% positive edges. Based on those networks, we characterized the nodes (taxa and metabolites) with the highest degree (i.e. number of connections; Fig. 5b,d). Notably, the top three

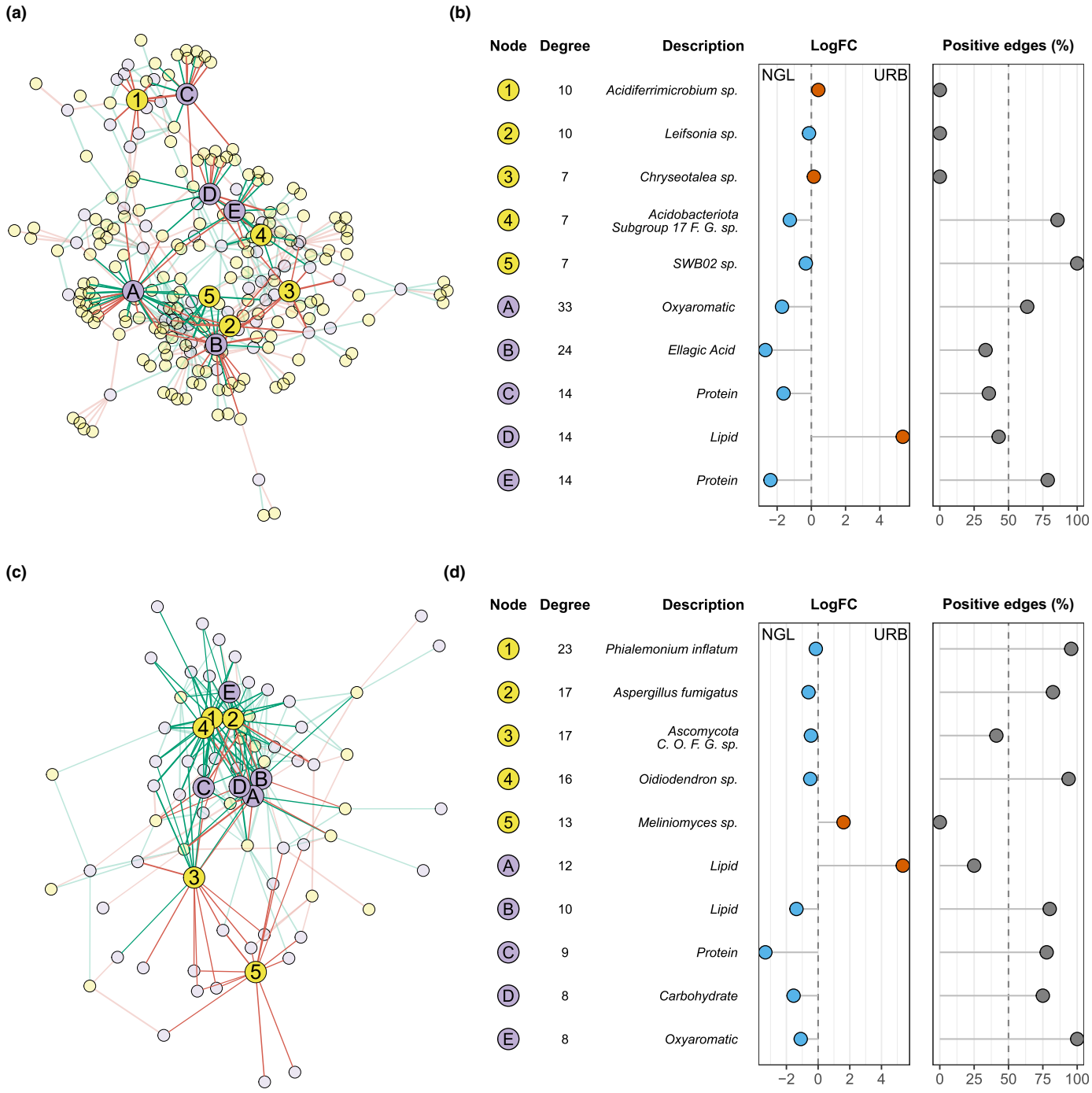

Fig. 5 Correlation analysis between key metabolites (purple) and prokaryotic and fungal taxa (yellow) in the rhizosphere of *Quercus* spp. Spearman partial correlation network of prokaryotic (a) and fungal (c) microbiomes and key metabolites. Network edges represent pairwise associations (Spearman's $\rho > 0.4$) between microbes and metabolites, but without statistical significance. Positive correlations are indicated by green edges while negative correlations are indicated by red edges. Characterization of the top five connected metabolites and prokaryotic (b) and fungal (d) amplicon sequence variants. Shown are their degree (number of correlations with correlation coefficient > 0.4), taxonomic classification or assigned metabolite class, their abundance $\log_2$ fold change between the origins (negative $\log_2$FC indicates enrichment in origin north German lowland NGL, positive $\log_2$FC indicates enrichment at origin upper Rhine basin URB). The 'Positive edges [%]' column represents the proportion of positive correlations relative to the total degree of the node.

bacterial taxa with the highest number of strong correlations, *Acidiferrimicrobium* sp. (degree = 10), *Leifsonia* sp. (10), and *Chryseotalea* sp. (degree = 7) showed only negative correlations with metabolites. The other two bacterial taxa, one from the phylum *Acidobacteriota* (degree = 7) and one from the genus SWB0 from the family *Hyphomonadaceae* (degree = 7), showed mostly

positive correlations (85.7% and 100%). None of the top connected taxa showed significant differential abundance between the origins (Fig. 5b column Log_2FC).

Notably, ellagic acid was the metabolite with the second-highest degree in the prokaryotic network (24) and was also found within the top 10 metabolites with the highest VIP score. It was enriched in origin NGL with a log_2 fold change of −2.69 and showed 33.3% positive correlations. The other, not further classified, metabolites with a high degree were one oxyaromatic compound (degree = 33) and two proteins (both degree = 14), which were significantly enriched in origin NGL ($log_2FC = -1.62$ and −2.39) with positive edge percentages of 35.7% and 78.6%, respectively. Conversely, one lipid (degree = 14) that was strongly enriched in origin URB ($log_2FC = 5.35$) with a positive edge percentage of 42.9% was also within the top five connected nodes. This compound was annotated as an iridoid similar to plant-derived valeriotetrate.

For metabolite interactions with fungal ASVs, three of the ASVs with the highest degree, *P. inflatum* (degree = 23), *Aspergillus fumigatus* (degree = 17), and *Oidiodendron sp.* (degree = 16), showed mostly positive correlations with the metabolites (95.7%, 82.3%, and 93.8%). An ASV of phylum *Ascomycota* (degree = 17) and one of genus *Meliniomyces* (degree = 13) showed lower positive edge percentage (41.1% and 0.0%). None of the ASVs showed significant differential abundance between the origins (Fig. 5d column Log_2FC). Four metabolites, one from each of the following classes: lipids, proteins, carbohydrates, and oxyaromatic compounds, were enriched in NGL ($log_2FC = -1.37, -3.33, -1.55, -1.10$) and showed predominantly positive correlations (80.0%, 77.8%, 75.0%, 100%). Once again, there was one URB-enriched lipid in the top five connected metabolites ($log_2FC = 5.35$, degree = 12). This lipid was the same one already found in the prokaryotic network (Node D). It had a positive edge percentage of 25.0% in the fungal network.

iWUE impacts prokaryotic but not fungal composition and diversity

According to the experimental design, in which iWUE was implemented as an independent tree variable across sites, tree origin or species had no significant effect on this parameter (Table 1). Nevertheless, iWUE was slightly higher on average in trees originating from NGL compared to URB ($P = 0.078$). Spearman's rank correlation analysis revealed that trees with higher iWUE values had lower prokaryotic diversity in the rhizosphere microbiome. A significantly negative correlation was found between iWUE and both prokaryotic richness (rho = −0.50, $P = 0.002$) and Shannon diversity (rho = −0.60, $P = 0.002$, Fig. S7) across all samples (Fig. 6). This correlation was also observed for the NGL and *Q. robur* data subsets (Table 2). PERMANOVA revealed furthermore that iWUE of the tree significantly impacted the prokaryotic community composition ($R^2 = 0.04$, $P = 0.036$) (Fig. 2b). Within samples from the origin NGL, we found *Blastocatellaceae* ($log_2FC = 0.30$, $P = 0.024$) and *Micromonosporaceae* ($log_2FC = 0.47$, $P = 0.008$) to be positively associated with iWUE (DESeq2 results; Fig. 3).

We did not observe any significant relationship between richness and iWUE for fungal communities (Fig. 6). However, fungal evenness showed a significant negative relationship with iWUE (rho = −0.46, $P = 0.005$, not shown). While the fungal community composition did not differ significantly between tree species or seed origins, the interaction between origin and iWUE significantly affected it ($R^2 = 0.05$; $P = 0.014$, Fig. 2b). Finally, we could not associate fungal taxa or families with iWUE using DESeq2.

Table 1 Intrinsic water use efficiency (iWUE) average values and SD by oak (*Quercus* spp.) species and origin (upper rhine basin (URB) and north German lowlands (NGL)).

Species – Origin	iWUE (μmol mol^{-1})
Quercus robur – NGL	88.3 ± 13.2
Quercus petraea – NGL	92.9 ± 16.5
Quercus robur – URB	80.5 ± 22.0
Quercus petraea – URB	79.91 ± 16.24

Discussion

In the present study, we found that the origin of the *Q. petraea* and *Q. robur* seeds has an effect in the rhizosphere after years of growth under identical conditions, shaping its prokaryotic microbiome and metabolome. However, we observed neither significant species-specific effects on the oak rhizosphere nor a similar response from the fungal community. Furthermore, independently of origin, higher tree iWUE was significantly associated with lower prokaryotic alpha diversity in the rhizosphere.

Tree origin legacy effect on rhizosphere microbiome and metabolome

The origin of the seeds had a small but significant effect on the composition of the prokaryotic community. The compositional shift was characterized by the increase of the *Pseudonocardiaceae* diversity in the rhizosphere of trees originating from a relatively dry region, NGL, and an increase of *Sphingobacteriaceae* at URB, characterized by a higher precipitation level. The enrichment of *Pseudonocardiaceae* at the drier site is notable; this family, including genera such as *Pseudonocardia* and *Amycolatopsis*, is known for its drought tolerance and various plant growth-promoting traits (Borah & Thakur, 2020; Chaiya *et al.*, 2021; Xie *et al.*, 2024). Notably, some members of this family are described as endophytes, for example within the genus *Pseudonocardia* (Qin *et al.*, 2011). This lifestyle could facilitate the vertical microbiome transmission mentioned later. Furthermore, trees from the origin URB exhibited higher rhizosphere prokaryotic and fungal Shannon diversity. While the higher Shannon index of the prokaryotic community in URB was driven by higher richness, the fungal diversity difference was caused primarily by increased evenness.

The detection of differences in microbiome composition between origins aligns with previous research demonstrating that

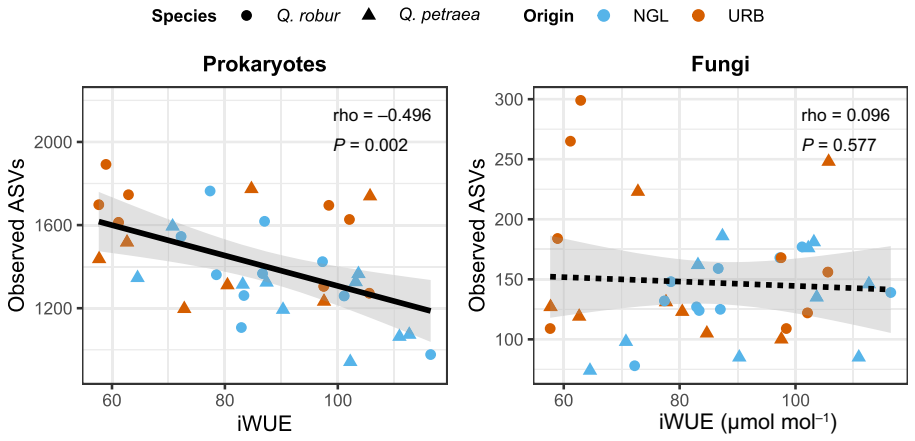

Fig. 6 Spearman correlation of microbial richness and intrinsic water use efficiency (iWUE) across tree species (*Quercus* spp.) but split between origin (upper Rhine basin, URB; north German lowland, NGL). Spearman correlation coefficient and *P*-values are indicated in the plot. Solid lines indicate significant correlation ($P \leq 0.05$), while dotted lines represent non-significant trends. Correlation between fungal evenness and iWUE was not significant.

Table 2 Spearman correlation between microbial richness and water use efficiency (iWUE) for oak (*Quercus* spp.) rhizosphere sample subsets split by origin (upper rhine basin (URB) and north German lowlands (NGL)). Rho denotes spearman rank correlation coefficient, df denotes degrees of freedom. Shown are unadjusted *P*-values. Asterisks denote statistical significance (*, $P \leq 0.05$; **, $P \leq 0.01$).

	Prokaryotes			Fungi		
	rho	df	*P*-value	rho	df	*P*-value
Full	−0.50	34	0.002**	0.07	34	0.577
NGL	−0.59	18	0.007**	0.41	18	0.073
URB	−0.18	14	0.498	−0.11	14	0.688
Quercus robur	−0.56	16	0.016*	−0.10	16	0.705
Quercus petraea	−0.43	16	0.076	0.26	16	0.291

seed or plant origin can shape tree microbiomes, such as prokaryotic endophytes and fungal rhizosphere communities (Färkkilä *et al.*, 2023; Maitra *et al.*, 2024). Our results are consistent with the results of recent work by Liu *et al.* (2024), who identified significant differences in the rhizosphere microbiomes among 11 provenances of *Fokienia hodginsii*. By demonstrating this phenomenon through a long-term experiment with a robust, biologically replicated design, our study corroborates their findings regarding an origin legacy effect.

We observed no differences in the composition of the fungal or prokaryotic communities between *Q. petraea* and *Q. robur*. This finding was surprising, since rhizosphere microbiome differences between different tree species can be expected to be stronger than between intraspecific ecotypes and are frequently described (Ishida *et al.*, 2007; Wang & Sugiyama, 2020). On the other hand, differences in the rhizosphere can be small and hard to detect and are often observed in adult trees (Cregger *et al.*, 2018; Bonito *et al.*, 2019). The ecogeographic adaptation to the region of origin might have overwritten the species-specific effects, especially considering the close relatedness of both species.

To investigate the potential drivers behind the origin legacy effect, we examined the rhizosphere metabolome as a link between the tree phenotype and microbiome composition. The metabolome composition mirrored the pattern that we observed in microbiomes. OPLS-DA separated metabolomes by origins but not by species. Interestingly, the metabolite alpha diversity was higher in trees from NGL, displaying a reverse trend of what was observed in the prokaryotic microbiome. Furthermore, the metabolite evenness was higher in *Q. petraea* than in *Q. robur*. While large environmental surveys often find positive metabolome–microbiome covariation (Shaffer *et al.*, 2022), we detected no global congruence (Procrustes) and found a negative association between prokaryotic and metabolite Shannon diversity. This divergence could reflect targeted exudation under drier conditions, metabolic channeling by subsets of taxa, or ontogenetic exudation traits in juveniles, as further discussed later.

Through exploratory correlation network analysis, we identified plant-derived ellagic acid as a potential mediator of drought adaptation. It was significantly enriched in the drier origin NGL and was highly correlated with a range of prokaryotic taxa. Ellagic acid is abundant in oaks (Othón-Díaz *et al.*, 2023). It can alleviate water-deficit stress via antioxidant pathways (García-Niño & Zazueta, 2015; Debnath *et al.*, 2020). For example, seed pretreatment with ellagic acid has been shown to enhance drought tolerance in seedlings of *Cicer arietinum* (chickpea) and *Brassica napus* (canola) (El-Soud *et al.*, 2013; Khan *et al.*, 2017). Furthermore, treating maize with ellagic acid effectively reduced drought stress symptoms (Agar *et al.*, 2024). Based on our results, ellagic acid may have another function via interactions with the rhizosphere microbiome. The other notable metabolite, which was strongly enriched in origin URB, was a valeriotetrate-like iridoid, a class of plant-derived compounds that are involved in defense against herbivores and pathogens (Bowers & Stamp, 1993; Biere *et al.*, 2004). Among microbes, *Leifsonia*, which is frequently found in the rhizosphere and is implicated in osmotic stress tolerance (Kang *et al.*, 2017; Nordstedt *et al.*, 2021), and

Phialemonium inflatum, which is reported to promote growth and suppress pathogens (Zhou *et al.*, 2018; Rivera-Vega *et al.*, 2022), were both connected to a high number of metabolites in the network analysis. As microbial communities shape rhizosphere chemistry themselves, these patterns likely reflect bidirectional feedback between exudation and microbial community structure, rather than unidirectional plant control.

Mechanistic routes for legacy persistence

Origin legacy effects in the rhizosphere microbiome can be mediated in two ways: vertical and horizontal transmission (Gundel *et al.*, 2011; Shade *et al.*, 2017). Vertical transmission, carryover of the microbiome from the mother tree via the seed, was previously seen in several plants, including oaks (Johnston-Monje & Raizada, 2011; Hardoim *et al.*, 2012; Walitang *et al.*, 2019; Abdelfattah *et al.*, 2021; Fort *et al.*, 2021). It is unclear whether the transmitted species could remain on the next generation of plants for up to 6 yr (Vandenkoornhuyse *et al.*, 2015). Horizontal transfer depends on the ability of ecotypes to adapt to their specific habitats. Such adaptation leads to genetic or epigenetic changes that are inherited across generations. Resulting variations in root morphology and exudation between tree ecotypes have been widely reported and could alter the recruitment of a specific microbiome from the bulk soil (Liu *et al.*, 2024; Luo *et al.*, 2017; Seitz *et al.*, 2022).

Here, it must be noted that the samples were collected from 6-yr-old trees, which were still in the juvenile stage of development. The root exudation patterns change significantly with tree development phase. Often, the total amount of exudates reduces with age, and the focus shifts from nutrient acquisition toward a greater investment in defensive capabilities (Chaparro *et al.*, 2013; Li *et al.*, 2021; Chen *et al.*, 2023). The selective pressure exerted by juveniles on their rhizosphere microbiome may be weaker, especially since the trees were subjected to minimal stress compared with natural environments. This may allow seed-transmitted communities to persist alongside the progressive horizontal acquisition of microbiomes. Both a strong origin adaptation and a weak exudative specificity at this juvenile stage could explain the lack of differences in microbiomes and metabolomes between species while accounting for origin-specific differences. Moreover, this might also put juvenile trees in a vulnerable position under climate change, being dependent on their parent trait transfer for successful survival during early growth stages (Au *et al.*, 2022).

Ultimately, knowledge of the original seed microbiome and analysis of root exudation (and other phenotypic or genotypic parameters) could help to clarify how the origin legacy effect is mediated in oaks.

Rhizosphere fungal microbiome is less sensitive to plant traits and origin than the prokaryotic microbiome

Although the seed origin and iWUE were reflected in prokaryotic microbiomes, the fungal rhizosphere showed no comparable effects of origin, species or iWUE, and displayed fewer metabolite interactions. This result also held for ECM fungi (primarily the typical oak symbionts from genus *Scleroderma* (Bzdyk *et al.*, 2018)), despite the frequent host specificity reported for this guild (Ishida *et al.*, 2007). This is consistent with reports that the composition of ECM communities is often more influenced by environmental properties than by host traits (Karliński *et al.*, 2013; Downie *et al.*, 2021). As the soil conditions in our experiment were identical across trees, large differences in fungal composition were not anticipated. Furthermore, a potentially limited pool of available fungal taxa in the initial substrate could have limited recruitment, contributing to the lack of difference. This lack of host effects on the fungal microbiome may also be an instance of phylosymbiosis, as the close evolutionary relationship between the two oak hosts is likely reflected in the composition of their fungal symbionts. It should be noted that we did not capture arbuscular mycorrhizal fungi (AMF), likely due to the use of universal ITS primers, which are known to underrepresent AMF (Štůsková *et al.*, 2025).

Furthermore, several studies demonstrated stronger effects of host traits on bacteria than on fungi (Merino-Martín *et al.*, 2020; Gaete *et al.*, 2021; Ye *et al.*, 2021; Song *et al.*, 2025). Finally, fungi are generally more dispersal-limited than prokaryotes (Song *et al.*, 2025), which in turn contributes to higher intersample heterogeneity as rhizosphere communities assemble from a more localized soil environment (Collins *et al.*, 2018; Merino-Martín *et al.*, 2020; Zhang *et al.*, 2021). This increased variability can reduce the specificity of the fungal microbiome to its host.

Diversity of the rhizosphere microbial community is associated with tree intrinsic water-use efficiency

In our analysis, iWUE was a significant predictor of prokaryotic community composition (PERMANOVA, $R^2 = 4.0\%$) and was negatively correlated with prokaryotic alpha diversity. Thus, trees with higher iWUE harbored less diverse prokaryotic communities, regardless of the seed origin or species.

The rhizosphere microbiome can improve the host drought tolerance via alteration of root morphology, extension of the root system by fungal hyphae, exudation profiles, or stomatal conductance (Augé *et al.*, 2015; Kannenberg & Phillips, 2017; Carter *et al.*, 2023). The specific rhizosphere microbiome can therefore be seen as a dimension of drought tolerance adaptation (Ulrich *et al.*, 2019; Ben Zineb *et al.*, 2024). Consequently, Gaete *et al.* (2021) reported that the prokaryotic microbiomes of drought-tolerant and drought-susceptible tomato plants differ in their alpha diversity, beta diversity, and interaction network complexity. Contrary to our results, these differences were dependent on drought rather than being apparent under normal irrigation conditions.

Direct evidence linking iWUE and rhizosphere diversity remains limited and is likely to be context-dependent (Naylor & Coleman-Derr, 2018). We hypothesize that adaptation to drier conditions increases the specificity of exudate-mediated selection, yielding more specialized and less diverse microbiomes. The stronger correlation between iWUE and richness at NGL supports this hypothesis.

Within the trees originating from NGL, two prokaryotic families, *Blastocatellaceae* and *Micromonosporaceae*, were positively associated with iWUE. Members of both families have been previously found in plant rhizospheres. Although they had not yet been linked to drought tolerance or growth promotion in plants (Sun *et al.*, 2019; Ling *et al.*, 2022; Abdullaeva *et al.*, 2024; Long *et al.*, 2024), their affiliation with the stress-resilient groups *Acidobacteriota* and *Actinobacteria* (Lavallee *et al.*, 2024) makes them potential contributors to plant drought responses. We predict that the compositional differences between the rhizospheres of oak trees of different origins may become more pronounced under drought stress.

Conclusion and implications

Our data demonstrate the importance of ecotypic adaptation for the structure of the rhizosphere environment of oak trees. The origin of seeds leaves a lasting imprint on the metabolome and prokaryotic diversity and composition of oak rhizospheres, whereas species effects are minimal. Leaf iWUE, a trait associated with drought adaptation, covaries with these belowground features independently of the tree origin. This suggests the existence of a trait–microbiome axis that is relevant to drought resilience. The lack of a strong response from the fungal community indicates that prokaryotic and fungal communities in the rhizosphere are shaped by different ecological drivers.

In the face of climate change-driving rapid range shifts, assisted migration is a key forest adaptation strategy.

Given that assisted migration alone cannot completely prevent declines in forest ecosystem services, selecting trees based on origin or functional traits such as iWUE may be a more effective strategy than relying on species-level traits alone. As the effects observed in our experiment are modest yet consistent across biomes, they reveal parameters that can be used in process-based models to couple soil microbes with plant water/carbon exchange. Pairing provenance selection with a microbiome-aware approach offers a practical solution to the challenges of assisted migration and forest restoration in the context of global change.

While our conclusions are constrained by the juvenile stage of the oaks, the common-garden pot context, and the correlative nature of the study, they motivate targeted future research. To elucidate the mechanisms underlying the legacy effects and verify their functional relevance for drought tolerance, causal tests should be conducted, such as reciprocal microbiome transfers, mechanistic analyses of root exudation dynamics, and long-term ontogenetic tracking.

Together, these efforts will refine our understanding of how provenance and functional traits shape oak–microbiome systems, and inform provenance-aware, microbiome-informed strategies to enhance forest resilience.

Acknowledgements

This work has been supported by the grants 2220WK09A4 and 2220WK09B4 from the German Federal Ministry of Food and Agriculture (BMEL), Federal Ministry for the Environment, Nature Conservation and Nuclear Safety (BMU) in the frame of the Waldklimafonds Program. This study was additionally supported by the German Research Foundation (DFG) (Grant 457330647), as part of the Research Unit 5315. In addition, the large-language models Gemini (Google LLC) were used for language editing of the manuscript text and for assistance with formatting, refactoring, and debugging of R analysis scripts. All AI-generated code and text edits were subsequently reviewed and adapted by the authors. Open Access funding enabled and organized by Projekt DEAL.

Competing interests

None declared.

Author contributions

TN, HS, MS and JPS designed this study. TN, HS and BK conducted experiments. SB, TN, IZ, SS, FB and PBSB analyzed samples and interpreted the data. BK, HS and JPS administered the project. SB with support of TN wrote the manuscript, with input from all authors. All authors read and approved the final version of the manuscript.

ORCID

Sebastian Bibinger https://orcid.org/0009-0002-7878-0521
Franz Buegger https://orcid.org/0000-0003-3526-4711
Birgit Kersten https://orcid.org/0000-0001-9900-9133
Tetyana Nosenko https://orcid.org/0000-0002-2104-8631
Michael Schloter https://orcid.org/0000-0003-1671-1125
Jörg-Peter Schnitzler https://orcid.org/0000-0002-9825-867X
Hilke Schroeder https://orcid.org/0000-0002-0908-3397
Stefanie Schulz https://orcid.org/0000-0001-5520-8106
Prasath Balaji Sivaprakasam Padmanaban https://orcid.org/0000-0002-9735-7238
Ina Zimmer https://orcid.org/0000-0002-6441-8495

Data availability

The raw data (16S and ITS sequences) are available in the NCBI Sequence Read Archive (SRA) under accession no. PRJNA1354844. All processed datasets, including phyloseq objects, metabolite abundance matrices, and metadata required to reproduce the analysis, are archived on Zenodo (doi: 10.5281/zenodo.17514228). The R code used for sequence processing, statistical analysis, and figure generation is publicly available on GitHub (https://github.com/SebastianBibinger/Oak_provenance) and permanently archived on Zenodo (doi: 10.5281/zenodo.17514848).

References

Abarenkov K, Nilsson RH, Larsson KH, Taylor AFS, May TW, Frøslev TG, Pawlowska J, Lindahl B, Põldmaa K, Truong C *et al.* 2024. The UNITE

database for molecular identification and taxonomic communication of fungi and other eukaryotes: sequences, taxa and classifications reconsidered. *Nucleic Acids Research* **52**: D791–D797.

Abdelfattah A, Wisniewski M, Schena L, Tack AJM. 2021. Experimental evidence of microbial inheritance in plants and transmission routes from seed to phyllosphere and root. *Environmental Microbiology* **23**: 2199–2214.

Abdullaeva Y, Ratering S, Rosado-Porto D, Manirajan BA, Glatt A, Schnell S, Cardinale M. 2024. Domestication caused taxonomical and functional shifts in the wheat rhizosphere microbiota, and weakened the natural bacterial biocontrol against fungal pathogens. *Microbiological Research* **281**: 127601.

Agar G, Yagci Ergul S, Yuce M, Arslan Yuksel E, Aydin M, Taspinar MS. 2024. Ellagic acid alleviates aluminum and/or drought stress through morpho-physiochemical adjustments and stress-related gene expression in *Zea mays* L. *Environmental Science and Pollution Research International* **31**: 59521–59532.

Aitken SN, Bemmels JB. 2016. Time to get moving: assisted gene flow of forest trees. *Evolutionary Applications* **9**: 271–290.

Allen CD, Macalady AK, Chenchouni H, Bachelet D, McDowell N, Vennetier M, Kitzberger T, Rigling A, Breshears DD, Hogg EH *et al.* 2010. A global overview of drought and heat-induced tree mortality reveals emerging climate change risks for forests. *Forest Ecology and Management* **259**: 660–684.

Antonov M, Csárdi G, Horvát S, Müller K, Nepusz T, Noom D, Salmon M, Traag V, Welles BF, Zanini F. 2023. igraph enables fast and robust network analysis across programming languages. *arXiv*.

Apprill A, McNally S, Parsons R, Weber L. 2015. Minor revision to V4 region SSU rRNA 806R gene primer greatly increases detection of SAR11 bacterioplankton. *Aquatic Microbial Ecology* **75**: 129–137.

Arend M, Kuster T, Günthardt-Goerg MS, Dobbertin M. 2011. Provenance-specific growth responses to drought and air warming in three European oak species (*Quercus robur*, *Q. petraea* and *Q. pubescens*). *Tree Physiology* **31**: 287–297.

Au TF, Maxwell JT, Robeson SM, Li J, Siani SMO, Novick KA, Dannenberg MP, Phillips RP, Li T, Chen Z *et al.* 2022. Younger trees in the upper canopy are more sensitive but also more resilient to drought. *Nature Climate Change* **12**: 1168–1174.

Augé RM. 2001. Water relations, drought and vesicular-arbuscular mycorrhizal symbiosis. *Mycorrhiza* **11**: 3–42.

Augé RM, Toler HD, Saxton AM. 2015. Arbuscular mycorrhizal symbiosis alters stomatal conductance of host plants more under drought than under amply watered conditions: a meta-analysis. *Mycorrhiza* **25**: 13–24.

Belmecheri S, Lavergne A. 2020. Compiled records of atmospheric CO_2 concentrations and stable carbon isotopes to reconstruct climate and derive plant ecophysiological indices from tree rings. *Dendrochronologia* **63**: 125748.

Ben Zineb A, Lamine M, Khallef A, Hamdi H, Ahmed T, Al-Jabri H, Alsafran M, Mliki A, Sayadi S, Gargouri M. 2024. Harnessing rhizospheric core microbiomes from arid regions for enhancing date palm resilience to climate change effects. *Frontiers in Microbiology* **15**: 1362722.

Bertić M, Schroeder H, Kersten B, Fladung M, Orgel F, Buegger F, Schnitzler JP, Ghirardo A. 2021. European oak chemical diversity – from ecotypes to herbivore resistance. *New Phytologist* **232**: 818–834.

Biere A, Marak HB, Van Damme JMM. 2004. Plant chemical defense against herbivores and pathogens: generalized defense or trade-offs? *Oecologia* **140**: 430–441.

Blickensdörfer L, Oehmichen K, Pflugmacher D, Kleinschmit B, Hostert P. 2024. National tree species mapping using Sentinel-1/2 time series and German national forest inventory data. *Remote Sensing of Environment* **304**: 114069.

Bonito G, Benucci GMN, Hameed K, Weighill D, Jones P, Chen KH, Jacobson D, Schadt C, Vilgalys R. 2019. Fungal-bacterial networks in the *Populus* rhizobiome are impacted by soil properties and host genotype. *Frontiers in Microbiology* **10**: 481.

van den Boogaart KG, Tolosana-Delgado R, Bren M. 2024. *Compositions: compositional data analysis, v.2.0.8.* Freiberg, Germany: TU Bergakademie Freiberg. [WWW document] URL http://www.stat.boogaart.de/compositions/.

Borah A, Thakur D. 2020. Phylogenetic and functional characterization of culturable endophytic actinobacteria associated with *Camellia* spp. for growth promotion in commercial tea cultivars. *Frontiers in Microbiology* **11**: 514973.

Bowers MD, Stamp NE. 1993. Effects of plant age, genotype, and herbivory on *Plantago* performance and chemistry. *Ecology* **74**: 1778–1791.

Brendel O, Le Thiec D, Scotti-Saintagne C, Bodénès C, Kremer A, Guehl JM. 2008. Quantitative trait loci controlling water use efficiency and related traits in *Quercus robur* L. *Tree Genetics & Genomes* **4**: 263–278.

Brown SP, Grillo MA, Podowski JC, Heath KD. 2020. Soil origin and plant genotype structure distinct microbiome compartments in the model legume *Medicago truncatula*. *Microbiome* **8**: 133.

Bruker Daltonics. 2020. *Metaboscape,* v.*4.0.* Bremen, Germany: Bruker Daltonics GmbH & Co. KG. [WWW document] URL https://www.bruker.com.

Bruschi P. 2010. Geographical variation in morphology of *Quercus petraea* (Matt.) Liebl. as related to drought stress. *Plant Biosystems* **144**: 298–307.

Bulgarelli D, Schlaeppi K, Spaepen S, Van Themaat EVL, Schulze-Lefert P. 2013. Structure and functions of the bacterial microbiota of plants. *Annual Review of Plant Biology* **64**: 807–838.

Bzdyk RM, Olchowik J, Studnicki M, Oszako T, Sikora K, Szmidla H, Hilszczańska D. 2018. The impact of effective microorganisms (EM) and organic and mineral fertilizers on the growth and mycorrhizal colonization of *Fagus sylvatica* and *Quercus robur* seedlings in a bare-root nursery experiment. *Forests* **9**: 597.

Callahan BJ, McMurdie PJ, Rosen MJ, Han AW, Johnson AJA, Holmes SP. 2016. DADA2: high-resolution sample inference from Illumina amplicon data. *Nature Methods* **13**: 581–583.

Carter KR, Nachtsheim AC, Dickman LT, Moore ER, Negi S, Heneghan JP, Sabella AJ, Steadman CR, Albright MBN, Anderson-Cook CM *et al.* 2023. Drought conditioning of rhizosphere microbiome influences maize water use traits. *Plant and Soil* **492**: 587–604.

Chaiya L, Kumla J, Suwannarach N, Kiatsiriroat T, Lumyong S. 2021. Isolation, characterization, and efficacy of actinobacteria associated with arbuscular mycorrhizal spores in promoting plant growth of chili (*Capsicum flutescens* L.). *Microorganisms* **9**: 1274.

Chaparro JM, Badri DV, Vivanco JM. 2013. Rhizosphere microbiome assemblage is affected by plant development. *The ISME Journal* **8**: 790–803.

Chen IC, Hill JK, Ohlemüller R, Roy DB, Thomas CD. 2011. Rapid range shifts of species associated with high levels of climate warming. *Science* **333**: 1024–1026.

Chen M, Yao X, Cheng H, Fan A, Lin R, Wang X, Yang Y, Chen G. 2023. Changes in Chinese fir plantations root exudation strategies seasonally and as tree age. *Forest Ecology and Management* **545**: 121239.

Collins CG, Stajich JE, Weber SE, Pombubpa N, Diez JM. 2018. Shrub range expansion alters diversity and distribution of soil fungal communities across an alpine elevation gradient. *Molecular Ecology* **27**: 2461–2476.

da Costa PB, Benucci GMN, Chou MY, Van Wyk J, Chretien M, Bonito G. 2022. Soil origin and plant genotype modulate switchgrass aboveground productivity and root microbiome assembly. *MBio* **13**: e00079-22.

Cregger MA, Veach AM, Yang ZK, Crouch MJ, Vilgalys R, Tuskan GA, Schadt CW. 2018. The *Populus* holobiont: dissecting the effects of plant niches and genotype on the microbiome. *Microbiome* **6**: 1–14.

Davis NM, Proctor D, Holmes SP, Relman DA, Callahan BJ. 2017. Simple statistical identification and removal of contaminant sequences in marker-gene and metagenomics data. *bioRxiv*.

Debnath B, Singh WS, Das M, Goswami S, Manna K. 2020. Biodynamic activities of ellagic acid: a dietary polyphenol. *Journal of Nature and Science of Medicine* **3**: 83–90.

Downie J, Taylor AFS, Iason G, Moore B, Silvertown J, Cavers S, Ennos R. 2021. Location, but not defensive genotype, determines ectomycorrhizal community composition in scots pine (*Pinus sylvestris* L.) seedlings. *Ecology and Evolution* **11**: 4826–4842.

El-Soud WA, Hegab MM, AbdElgawad H, Zinta G, Asard H. 2013. Ability of ellagic acid to alleviate osmotic stress on chickpea seedlings. *Plant Physiology and Biochemistry* **71**: 173–183.

Färkkilä SMA, Valtonen A, Saravesi K, Anslan S, Markkola A, Kontunen-Soppela S. 2023. The effects of geographic origin and genotype on fungal diversity of silver birch (*Betula pendula*). *Fungal Ecology* **63**: 101241.

Farquhar GD, Ehleringer JR, Hubick KT. 1989. Carbon isotope discrimination and photosynthesis. *Annual Review of Plant Physiology and Plant Molecular Biology* **40**: 503–537.

Fort T, Pauvert C, Zanne AE, Ovaskainen O, Caignard T, Barret M, Compant S, Hampe A, Delzon S, Vacher C. 2021. Maternal effects shape the seed mycobiome in *Quercus petraea*. *New Phytologist* **230**: 1594–1608.

Furneaux B. 2020. *FUNGuildR: look up guild information for fungi, v.0.2.0.* Uppsala, Sweden: Uppsala University. [WWW document] URL https://github.com/brendanf/FUNGuildR.

Gaete A, Pulgar R, Hodar C, Maldonado J, Pavez L, Zamorano D, Pastenes C, González M, Franck N, Mandakovic D. 2021. Tomato cultivars with variable tolerances to water deficit differentially modulate the composition and interaction patterns of their rhizosphere microbial communities. *Frontiers in Plant Science* **12**: 688533.

Gallart M, Adair KL, Love J, Meason DF, Clinton PW, Xue J, Turnbull MH. 2018. Host genotype and nitrogen form shape the root microbiome of *Pinus radiata*. *Microbial Ecology* **75**: 419–433.

García-Niño WR, Zazueta C. 2015. Ellagic acid: pharmacological activities and molecular mechanisms involved in liver protection. *Pharmacological Research* **97**: 84–103.

Garnier S, Ross N, Rudis R, Camargo PA, Sciaini M, Scherer C. 2024. Viridis (Lite) – colorblind-friendly color maps for R, *v.*0.6.5. CRAN. [WWW document] URL https://sjmgarnier.github.io/viridis/.

Ghirardo A, Lindstein F, Koch K, Buegger F, Schloter M, Albert A, Michelsen A, Winkler JB, Schnitzler JP, Rinnan R. 2020. Origin of volatile organic compound emissions from subarctic tundra under global warming. *Global Change Biology* **26**: 1908–1925.

Gieger T, Thomas FM. 2005. Differential response of two central-European oak species to single and combined stress factors. *Trees-Structure and Function* **19**: 607–618.

Gundel PE, Rudgers JA, Ghersa CM. 2011. Incorporating the process of vertical transmission into understanding of host–symbiont dynamics. *Oikos* **120**: 1121–1128.

Hansen MC, Potapov PV, Moore R, Hancher M, Turubanova SA, Tyukavina A, Thau D, Stehman SV, Goetz SJ, Loveland TR *et al.* 2013. High-resolution global maps of 21st-century forest cover change. *Science* **342**: 850–853.

Hardoim PR, Hardoim CCP, van Overbeek LS, van Elsas JD. 2012. Dynamics of seed-borne rice endophytes on early plant growth stages. *PLoS ONE* **7**: e30438.

Harrell F Jr. 2026. *Hmisc: Harrell Miscellaneous.* R package version 5.2-6. [WWW document] URL https://github.com/harrelfe/hmisc.

Hemmler D, Heinzmann SS, Wöhr K, Schmitt-Kopplin P, Witting M. 2018. Tandem HILIC-RP liquid chromatography for increased polarity coverage in food analysis. *Electrophoresis* **39**: 1645–1653.

Ishida TA, Nara K, Hogetsu T. 2007. Host effects on ectomycorrhizal fungal communities: insight from eight host species in mixed conifer-broadleaf forests. *New Phytologist* **174**: 430–440.

Johnston-Monje D, Raizada MN. 2011. Conservation and diversity of seed associated endophytes in *Zea* across boundaries of evolution, ethnography and ecology. *PLoS ONE* **6**: e20396.

Kang SM, Waqas M, Hamayun M, Asaf S, Khan AL, Kim AY, Park YG, Lee IJ. 2017. Gibberellins and indole-3-acetic acid producing rhizospheric bacterium *Leifsonia xyli* SE134 mitigates the adverse effects of copper-mediated stress on tomato. *Journal of Plant Interactions* **12**: 373–380.

Kannenberg SA, Phillips RP. 2017. Soil microbial communities buffer physiological responses to drought stress in three hardwood species. *Oecologia* **183**: 631–641.

Karliński L, Rudawska M, Leski T. 2013. The influence of host genotype and soil conditions on ectomycorrhizal community of *poplar* clones. *European Journal of Soil Biology* **58**: 51–58.

Kassambara A. 2023. ggpubr: 'ggplot2' based publication ready plots, v.0.6.0. CRAN. [WWW document] URL https://rpkgs.datanovia.com/ggpubr/.

Kembel SW, Cowan PD, Helmus MR, Cornwell WK, Morlon H, Ackerly DD, Blomberg SP, Webb CO. 2010. Picante: R tools for integrating phylogenies and ecology. *Bioinformatics* **26**: 1463–1464.

Khan A, Nazar S, Lang I, Nawaz H, Hussain MA. 2017. Effect of ellagic acid on growth and physiology of canola (*Brassica napus* L.) under saline conditions. *Journal of Plant Interactions* **12**: 520–525.

Koprivova A, Kopriva S. 2022. Plant secondary metabolites altering root microbiome composition and function. *Current Opinion in Plant Biology* **67**: 102227.

Kuster TM, Arend M, Günthardt-Goerg MS, Schulin R. 2013. Root growth of different oak provenances in two soils under drought stress and air warming conditions. *Plant and Soil* **369**: 61–71.

Lahti L, Shetty S. 2017. *Microbiome: R package, v.1.28.0.* Turku, Finland: University of Turku. [WWW document] URL http://microbiome.github.io.

Lamit LJ, Holeski LM, Flores-Rentería L, Whitham TG, Gehring CA. 2016. Tree genotype influences ectomycorrhizal fungal community structure: ecological and evolutionary implications. *Fungal Ecology* **24**: 124–134.

Lavallee JM, Chomel M, Alvarez Segura N, de Castro F, Goodall T, Magilton M, Rhymes JM, Delgado-Baquerizo M, Griffiths RI, Baggs EM *et al.* 2024. Land management shapes drought responses of dominant soil microbial taxa across grasslands. *Nature Communications* **15**: 29.

Le Provost G, Gerardin T, Plomion C, Brendel O. 2022. Molecular plasticity to soil water deficit differs between sessile oak (*Quercus petraea* (Matt.) Liebl.) high- and low-water use efficiency genotypes. *Tree Physiology* **42**: 2546–2562.

Lekberg Y, Schnoor T, Kjøller R, Gibbons SM, Hansen LH, Al-Soud WA, Sørensen SJ, Rosendahl S. 2012. 454-sequencing reveals stochastic local reassembly and high disturbance tolerance within arbuscular mycorrhizal fungal communities. *Journal of Ecology* **100**: 151–160.

Li Y, Wu X, Chen T, Wang W, Liu G, Zhang W, Li S, Wang M, Zhao C, Zhou H *et al.* 2018. Plant phenotypic traits eventually shape its microbiota: a common garden test. *Frontiers in Microbiology* **9**: 2479.

Li Z, Liu Z, Gao G, Yang X, Gu J. 2021. Shift from acquisitive to conservative root resource acquisition strategy associated with increasing tree age: a case study of *Fraxinus mandshurica*. *Forests* **12**: 1797.

Ling N, Wang T, Kuzyakov Y. 2022. Rhizosphere bacteriome structure and functions. *Nature Communications* **13**: 1–13.

Liu C, Cui Y, Li X, Yao M. 2021. Microeco: an R package for data mining in microbial community ecology. *FEMS Microbiology Ecology* **97**: fiaa255.

Liu HL, Zhu T, Wen X, Zhao Q, Chen Y, Wang YZ, Li J, Su S. 2024. Chemical and microbial differences of root and rhizosphere soil among different provenances of *Fokienia hodginsii*. *Forests* **15**: 1005.

Loarie SR, Duffy PB, Hamilton H, Asner GP, Field CB, Ackerly DD. 2009. The velocity of climate change. *Nature* **462**: 1052–1055.

Long PL, Fu L, Xiao Y, Gao J. 2024. *Micromonospora cathayae* sp. nov., isolated from the rhizosphere soil of *Cathaya argyrophylla*. *International Journal of Systematic and Evolutionary Microbiology* **74**: 006332.

Love MI, Huber W, Anders S. 2014. Moderated estimation of fold change and dispersion for RNA-seq data with DESeq2. *Genome Biology* **15**: 550.

Luo Q, Wang S, Sun LN, Wang H. 2017. Metabolic profiling of root exudates from two ecotypes of *Sedum alfredii* treated with Pb based on GC-MS. *Scientific Reports* **7**: 39878.

Maitra P, Hrynkiewicz K, Szuba A, Niestrawska A, Mucha J. 2024. The effects of *Pinus sylvestris* L. geographical origin on the community and co-occurrence of fungal and bacterial endophytes in a common garden experiment. *Microbiology Spectrum* **12**: e00807.

Manning C, Widmann M, Bevacqua E, Van Loon AF, Maraun D, Vrac M. 2019. Increased probability of compound long-duration dry and hot events in Europe during summer (1950-2013). *Environmental Research Letters* **14**: 094006.

Martin M. 2011. Cutadapt removes adapter sequences from high-throughput sequencing reads. *EMBnet Journal* **17**: 10.

Mathias JM, Hudiburg TW. 2022. IsocalcR: an R package to streamline and standardize stable isotope calculations in ecological research. *Global Change Biology* **28**: 7428–7436.

Merino-Martín L, Griffiths RI, Gweon HS, Furget-Bretagnon C, Oliver A, Mao Z, Le Bissonnais Y, Stokes A. 2020. Rhizosphere bacteria are more strongly related to plant root traits than fungi in temperate montane forests: insights from closed and open forest patches along an elevational gradient. *Plant and Soil* **450**: 183–200.

Mikryukov V. 2025. *MetagMisc: miscellaneous functions for metagenomic analysis.* GitHub.

Mukherjee S, Mishra AK. 2021. Increase in compound drought and heatwaves in a warming world. *Geophysical Research Letters* **48**: e2020GL090617.

Murphy K, Viroli C, Gormley IC. 2020. Infinite mixtures of infinite factor analysers. *Bayesian Analysis* **15**: 937–963.

Naylor D, Coleman-Derr D. 2018. Drought stress and root-associated bacterial communities. *Frontiers in Plant Science* **8**: 2223.

Nguyen NH, Song Z, Bates ST, Branco S, Tedersoo L, Menke J, Schilling JS, Kennedy PG. 2016. FUNGuild: an open annotation tool for parsing fungal community datasets by ecological guild. *Fungal Ecology* **20**: 241–248.

Nordstedt NP, Roman-Reyna V, Jacobs JM, Jones ML. 2021. Comparative genomic understanding of gram-positive plant growth-promoting *Leifsonia*. *Phytobiomes Journal* **5**: 263–274.

Nosenko T, Schroeder H, Zimmer I, Buegger F, Orgel F, Burau I, Padmanaban PBS, Ghirardo A, Bracker R, Kersten B *et al.* 2025. Patterns of adaptation to drought in *Quercus robur* populations in Central European temperate forests. *Global Change Biology* **31**: e70168.

Oksanen J, Simpson GL, Blanchet FG, Kindt R, Legendre P, Minchin PR, O'Hara RB, Solymos P, Stevens MHH, Szoecs E *et al.* 2025. *vegan: community ecology package, v.2.6.10.* Oulu, Finland: University of Oulu. [WWW document] URL https://vegandevs.github.io/vegan/.

Othón-Díaz ED, Fimbres-García JO, Flores-Sauceda M, Silva-Espinoza BA, López-Martínez LX, Bernal-Mercado AT, Ayala-Zavala JF. 2023. Antioxidants in oak (*Quercus* sp.): potential application to reduce oxidative rancidity in foods. *Antioxidants* **12**: 861.

Parada AE, Needham DM, Fuhrman JA. 2016. Every base matters: assessing small subunit rRNA primers for marine microbiomes with mock communities, time series and global field samples. *Environmental Microbiology* **18**: 1403–1414.

Pereira SIA, Abreu D, Moreira H, Vega A, Castro PML. 2020. Plant growth-promoting rhizobacteria (PGPR) improve the growth and nutrient use efficiency in maize (*Zea mays* L.) under water deficit conditions. *Heliyon* **6**: e05106.

Pfenninger M, Reuss F, KIebler A, Schönnenbeck P, Caliendo C, Gerber S, Cocchiararo B, Reuter S, Blüthgen N, Mody K *et al.* 2024. Correction: genomic basis for drought resistance in European beech forests threatened by climate change. *eLife* **13**: e102872.

Ponton S, Dupouey JL, Bréda N, Dreyer E. 2002. Comparison of water-use efficiency of seedlings from two sympatric oak species: genotype × environment interactions. *Tree Physiology* **22**: 413–422.

Ponton S, Dupouey JL, Bréda N, Feuillat F, Bodénès C, Dreyer E. 2001. Carbon isotope discrimination and wood anatomy variations in mixed stands of *Quercus robur* and *Quercus petraea*. *Plant, Cell & Environment* **24**: 861–868.

Qin S, Xing K, Fei SM, Lin Q, Chen XM, Cao CL, Sun Y, Wang Y, Li WJ, Jiang JH. 2011. *Pseudonocardia sichuanensis* sp. nov., a novel endophytic actinomycete isolated from the root of *Jatropha curcas* L. *Antonie van Leeuwenhoek International Journal of General and Molecular Microbiology* **99**: 395–401.

Quast C, Pruesse E, Yilmaz P, Gerken J, Schweer T, Yarza P, Peplies J, Glöckner FO. 2013. The SILVA ribosomal RNA gene database project: improved data processing and web-based tools. *Nucleic Acids Research* **41**: D590–D596.

R Core Team. 2024. *R: a language and environment for statistical computing, v.4.4.2.* Vienna, Austria: R Foundation for Statistical Computing. [WWW document] URL https://www.R-project.org/.

Rabarijaona A, Ponton S, Bert D, Ducousso A, Richard B, Levillain J, Brendel O. 2022. Provenance differences in water-use efficiency among sessile oak populations grown in a mesic common garden. *Frontiers in Forests and Global Change* **5**: 914199.

Rivas-Ubach A, Liu Y, Bianchi TS, Tolić N, Jansson C, Paša-Tolić L. 2018. Moving beyond the Van Krevelen diagram: a new stoichiometric approach for compound classification in organisms. *Analytical Chemistry* **90**: 6152–6160.

Rivera-Vega LJ, Grunseich JM, Aguirre NM, Valencia CU, Sword GA, Helms AM. 2022. A beneficial plant-associated fungus shifts the balance toward plant growth over resistance, increasing cucumber tolerance to root herbivory. *Plants* **11**: 282.

Rolli E, Marasco R, Vigani G, Ettoumi B, Mapelli F, Deangelis ML, Gandolfi C, Casati E, Previtali F, Gerbino R *et al.* 2015. Improved plant resistance to drought is promoted by the root-associated microbiome as a water stress-dependent trait. *Environmental Microbiology* **17**: 316–331.

RStudio Team. 2020. *RStudio: Integrated Development for R.* Boston, MA, USA: RStudio, PBC.

RStudio Team. 2023. *RStudio: integrated development environment for R, v.2023.09.1.* Boston, MA: Posit Software, PBC. [WWW document] URL http://www.posit.co/.

Scharnweber T, Manthey M, Criegee C, Bauwe A, Schröder C, Wilmking M. 2011. Drought matters – declining precipitation influences growth of *Fagus sylvatica* L. and *Quercus robur* L. in north-eastern Germany. *Forest Ecology and Management* **262**: 947–961.

Schlaeppi K, Dombrowski N, Oter RG, Ver Loren Van Themaat E, Schulze-Lefert P. 2014. Quantitative divergence of the bacterial root microbiota in *Arabidopsis thaliana* relatives. *Proceedings of the National Academy of Sciences, USA* **111**: 585–592.

Schroeder H, Kersten B. 2023. A small set of nuclear markers for reliable differentiation of the two closely related oak species *Quercus robur* and *Q. petraea*. *Plants* **12**: 566.

Seitz VA, McGivern BB, Daly RA, Chaparro JM, Borton MA, Sheflin AM, Kresovich S, Shields L, Schipanski ME, Wrighton KC *et al.* 2022. Variation in root exudate composition influences soil microbiome membership and function. *Applied and Environmental Microbiology* **88**: e00226-22.

Shade A, Jacques MA, Barret M. 2017. Ecological patterns of seed microbiome diversity, transmission, and assembly. *Current Opinion in Microbiology* **37**: 15–22.

Shaffer JP, Nothias LF, Thompson LR, Sanders JG, Salido RA, Couvillion SP, Brejnrod AD, Lejzerowicz F, Haiminen N, Huang S *et al.* 2022. Standardized multi-omics of Earth's microbiomes reveals microbial and metabolite diversity. *Nature Microbiology* **7**: 2128–2150.

Simon J, Dong F, Buegger F, Rennenberg H. 2013. Effects of Rhizospheric NO on N Uptake in Scots Pine. Plant Cell Environ. *Plant, Cell & Environment* **36**: 1019–1026.

Simonin M, Briand M, Chesneau G, Rochefort A, Marais C, Sarniguet A, Barret M. 2022. Seed microbiota revealed by a large-scale meta-analysis including 50 plant species. *New Phytologist* **234**: 1448–1463.

Simonin M, Dasilva C, Terzi V, Ngonkeu ELM, DIouf D, Kane A, Béna G, Moulin L. 2020. Influence of plant genotype and soil on the wheat rhizosphere microbiome: evidences for a core microbiome across eight African and European soils. *FEMS Microbiology Ecology* **96**: fiaa067.

Sivaprakasam Padmanaban PB, Stange P, Weber B, Pritsch K, Kark T, Benz PJ, Rosenkranz M, Schnitzler J-P. 2025. Strain and contact-dependent metabolomic reprogramming reveals distinct interaction strategies between *Laccaria bicolor* and *Trichoderma*. *Fungal Biology and Biotechnology* **12**: 13.

Song S, Yang X, Tang R, Zhang Y, Tang Z. 2025. Soil properties and plant functional traits have different importance in shaping rhizosphere soil bacterial and fungal communities in a meadow steppe. *mSystems* **10**: e00570-25.

Štůsková K, Vavříník A, Hakalová E, Čechová J, Gramaje D, Eichmeier A. 2025. Arbuscular mycorrhizal fungi strongly influence the endorhizosphere of grapevine rootstock with soil type as a key factor. *Mycorrhiza* **35**: Article 17.

Sun Y, Jiang ZM, Zhao LL, Su J, Yu LY, Tian YQ, Zhang YQ. 2019. *Allorhizocola rhizosphaerae* gen. nov., sp. nov., a new member of *Micromonosporaceae* isolated from rhizosphere soil of the plant *Calligonum mongolicum*. *International Journal of Systematic and Evolutionary Microbiology* **69**: 109–115.

Thevenot EA, Roux A, Xu Y, Ezan E, Junot C. 2015. Analysis of the human adult urinary metabolome variations with age, body mass index and gender by implementing a comprehensive workflow for univariate and OPLS statistical analyses. *Journal of Proteome Research* **14**: 3322–3335.

Thom D, Buras A, Heym M, Klemmt HJ, Wauer A. 2023. Varying growth response of Central European tree species to the extraordinary drought period of 2018–2020. *Agricultural and Forest Meteorology* **338**: 109506.

Thünen-Institut. 2022. Vierte Bundeswaldinventur – Ergebnisdatenbank. *bwi.info.*

Trivedi P, Leach JE, Tringe SG, Sa T, Singh BK. 2020. Plant–microbiome interactions: from community assembly to plant health. *Nature Reviews Microbiology* **18**: 607–621.

Ulrich DEM, Sevanto S, Ryan M, Albright MBN, Johansen RB, Dunbar JM. 2019. Plant-microbe interactions before drought influence plant physiological responses to subsequent severe drought. *Scientific Reports* **9**: 1–10.

U'Ren JM, Zimmerman NB. 2021. Oaks provide new perspective on seed microbiome assembly. *New Phytologist* **230**: 1293–1295.

Vandenkoornhuyse P, Quaiser A, Duhamel M, Le Van A, Dufresne A. 2015. The importance of the microbiome of the plant holobiont. *New Phytologist* **206**: 1196–1206.

Velmala SM, Rajala T, Haapanen M, Taylor AFS, Pennanen T. 2013. Genetic host-tree effects on the ectomycorrhizal community and root characteristics of Norway spruce. *Mycorrhiza* **23**: 21–33.

Vurukonda SSKP, Vardharajula S, Shrivastava M, SkZ A. 2016. Enhancement of drought stress tolerance in crops by plant growth promoting rhizobacteria. *Microbiological Research* **184**: 13–24.

Wagner MR, Lundberg DS, Del Rio TG, Tringe SG, Dangl JL, Mitchell-Olds T. 2016. Host genotype and age shape the leaf and root microbiomes of a wild perennial plant. *Nature Communications* **7**: 12151.

Walitang DI, Kim CG, Jeon S, Kang Y, Sa T. 2019. Conservation and transmission of seed bacterial endophytes across generations following crossbreeding and repeated inbreeding of rice at different geographic locations. *MicrobiologyOpen* **8**: e662.

Wang B, Sugiyama S. 2020. Phylogenetic signal of host plants in the bacterial and fungal root microbiomes of cultivated angiosperms. *The Plant Journal* **104**: 522–531.

Wang X, Zhang J, Lu X, Bai Y, Wang G. 2024. Two diversities meet in the rhizosphere: root specialized metabolites and microbiome. *Journal of Genetics and Genomics* **51**: 467–478.

Werner RA, Brand WA. 2001. Referencing strategies and techniques in stable isotope ratio analysis. *Rapid Communications in Mass Spectrometry* **15**: 501–519.

White TJ, Bruns T, Lee S, Taylor J. 1990. Amplification and direct sequencing of fungal ribosomal RNA genes for phylogenetics. In: *PCR protocols: a guide to methods and applications*. San Diego, CA, USA: Academic Press, 315–322.

Whitham TG, Gehring CA, Lamit LJ, Wojtowicz T, Evans LM, Keith AR, Smith DS. 2012. Community specificity: life and afterlife effects of genes. *Trends in Plant Science* **17**: 271–281.

Wickham H. 2016. *Ggplot2: elegant graphics for data analysis*. New York, NY, USA: Springer-Verlag.

Xie F, Andrews B, Asenjo JA, Goodfellow M, Pathom-aree W. 2024. Atacama Desert actinomycetes: taxonomic analysis, drought tolerance and plant growth promoting potential. *World Journal of Microbiology and Biotechnology* **40**: 1–20.

Ye F, Wang X, Wang Y, Wu S, Wu J, Hong Y. 2021. Different pioneer plant species have similar rhizosphere microbial communities. *Plant and Soil* **464**: 165–181.

Zhang G, Wei G, Wei F, Chen Z, He M, Jiao S, Wang Y, Dong L, Chen S. 2021. Dispersal limitation plays stronger role in the community assembly of fungi relative to bacteria in rhizosphere across the arable area of medicinal plant. *Frontiers in Microbiology* **12**: 713523.

Zhou W, Wheeler TA, Starr JL, Valencia CU. 2018. A fungal endophyte defensive symbiosis affects plant-nematode interactions in cotton. *Plant and Soil* **422**: 251–266.

Zou Y, Backus GA, Safford HD, Sawyer S, Baskett ML. 2024. Quantifying the capacity for assisted migration to achieve conservation and forestry goals under climate change. *Journal of Biogeography* **51**: 2440–2455.

Supporting Information

Additional Supporting Information may be found online in the Supporting Information section at the end of the article.

Fig. S1 Rhizosphere sampling method.

Fig. S2 Microbiome rarefaction curves.

Fig. S3 Bacterial and fungal community composition.

Fig. S4 Fungal guild classification.

Fig. S5 Key metabolite abundance.

Fig. S6 Correlation of microbial Shannon diversity and intrinsic water use efficiency (iWUE).

Fig. S7 Correlation of microbial and metabolite Shannon diversity.

Table S1 Origin climatic information.

Table S2 Soil properties at common garden.

Table S3 δ13C and iWUE for all used trees.

Table S4 16S read number during DADA2 pipeline.

Table S5 ITS read number during DADA2 pipeline.

Table S6 Summary of statistical test results for diversity and composition.

Table S7 Taxonomy of ASVs removed as contaminants.

Table S8 Microbiome PERMANOVA results.

Table S9 Key metabolites found through OPLS-DA.